Selective inhibition of partial EMT-induced tumour cell growth by cerium valence states of extracellular ceria nanoparticles for anticancer treatment

Tamaki Naganuma[*]

[*] *Research Center for Macromolecules and Biomaterials, National Institute for Materials Science, 1-1 Namiki, Tsukuba, Ibaraki, 305-0044, Japan. NAGANUMA.Tamaki@nims.go.jp; Tel: +81-298-60-4800. Fax: +81-298-60-4799*

ABSTRACT:

Targeting specific tumour cells and their microenvironments is essential for enhancing the efficacy of chemotherapy and reducing its side effects. A partial epithelial-to-mesenchymal transition state (pEMT, with a hybrid epithelial/mesenchymal phenotype) in tumour cells is an attractive targeting for anticancer treatment because it potentially provides maximal stemness and metastasis relevant to malignant cancer stem cell-like features. However, treatment strategies to target pEMT in tumour cells remain a challenge. This study demonstrates that extracellular cerium oxide nanoparticles (CNPs) selectively inhibit the growth of pEMT-induced tumour cells, without affecting full epithelial tumour cells. Herein, highly concentrated Ce^{3+} and Ce^{4+} ions are formed on CNP-layered poly-L-lactic acid surfaces. Cell cultures of pEMT-induced and uninduced lung cancer cell lines on the CNP-layered substrates allow the effect of extracellular CNPs on tumour cell growth to be investigated. The extracellular CNPs with dominant Ce^{3+} and Ce^{4+} ions were able to trap pEMT-induced tumour cells in a growth-arrested quiescent/dormant or cytostatic state without generating redox-related reactive oxygen species (ROS), i.e. non-redox mechanisms. The dominant Ce^{3+} state provided highly efficient growth inhibition of the pEMT-induced tumour cells. In contrast, the dominant Ce^{4+} state showed highly selective and appropriate growth regulation of normal and tumour cells, including a mesenchymal phenotype. Furthermore, Ce^{4+}-CNPs readily adsorbed serum-derived fibronectin and laminin. Cerium valence-specific proteins adsorbed on CNPs may influence receptor-mediated cell-CNP interactions, leading to tumour cell growth inhibition. These findings provide new perspectives for pEMT-targeting anticancer treatments based on the unique biointerface of extracellular CNPs with different Ce valence states.

KEYWORDS: Partial-EMT; Metal valence states; Nanoparticles; Mesenchymal phenotype; Non-redox mechanism; Anticancer treatment.

1. Introduction

Epithelial-to-mesenchymal transition (EMT) in cancer is a critical process to acquire cellular motility, leading to metastasis, stemness and drug resistance. In tumour cells, a partial EMT (pEMT) state, i.e. a hybrid epithelial/mesenchymal phenotype, correlates with maximal stemness and metastasis relevant to malignant cancer stem cell-like features [1–4]. Therapeutic targeting of the pEMT state is, therefore, a potential strategy to effectively overcome the poor prognosis conferred by pEMT [5,6]. However, EMT in human cancers is associated with different transition states, such as gradient pEMT states, with different tumour subpopulations [1,7]. Therapeutic approaches to target tumour cells undergoing pEMT, thus, are currently limited.

Nanotechnology for cancer treatment has advanced by using various nanoparticles (NPs) as drug delivery platforms, such as nanocarriers for anticancer drugs that target tumours [8,9]. Various targeting strategies to passively and actively accumulate NPs in solid tumours have been proposed, including passive tumour-tissue targeting (e.g. size/shape/charge-controlled NPs by enhanced permeability and retention (EPR) effect [10]), active tumour cell-specific targeting (e.g. functionalising NPs with tumour-specific ligands, such as antibodies, peptides and folic acid [8,9]), active biomimetic targeting (e.g. covering NPs with cell membranes derived from cancer, blood or stem cells [11,12]), and active organelle-targeting [13,14]. Moreover, to further enhance the targeting ability and therapeutic efficacy, hierarchical targeting, which is combined with multiple active and passive targeting strategies in response to variations of endogenous pH and redox stimuli and exogenous optical, thermal or magnetic stimuli, has attracted increasing attention [10]. Recently, the EPR effect in passive targeting has been recognised to be highly heterogeneous [10]. In addition, EPR-mediated accumulation may not recapitulate naturally occurring human solid tumours [15]. In contrast, active tumour cell-specific targeting can effectively enhance therapeutic

efficacy and cellular internalisation of nanomedicines [10,16]. However, several fundamental issues remain, and identifying an efficient design of NPs through their fixed physicochemical features to accomplish satisfying outcomes in all phases of tumour targeting may be impractical [10]. Nonetheless, targeting specific tumour cells and microenvironments is essential for enhancing anticancer treatments, such as enhancing the therapeutic efficacy of chemotherapy and reducing its side effects [2,17]. Most of the target ligands or receptors displayed on the cell membrane and their surroundings are derived from tumours and normal tissues, leading to adverse effects. Therefore, the complexities of tumour-specific ligands on cell membranes and tumour microenvironments contribute to the difficulty of developing effective treatments with reduced side effects [18,19].

Cerium oxide nanoparticles (CNPs) play an important role in reconciling divergent therapies that simultaneously provide apoptosis induction in tumours and avoid serious adverse events in normal tissues. Due to redox reactions between Ce^{4+} and Ce^{3+} ions, CNPs mimic several enzymatic activities and are accordingly referred to as "nanozymes" [20–22]. The therapeutic potential for CNPs has been increasing for various diseases, including atherosclerosis [23], multiple sclerosis [24], and Alzheimer's disease [25]. Notably, due to the pH discrepancy in the pathophysiological and physiological conditions, the enzyme-mimicking activities of CNPs potentially tune the production of toxic reactive oxygen species (ROS) in the weakly acidic microenvironment of tumours and the efficient scavenging of ROS in the neutral/weakly basic microenvironment of normal tissues. For instance, the antioxidant activity of CNPs prevents chemotherapy-induced acute kidney injury and myocardial damage, as well as radiotherapy-mediated side-effects in normal tissues [26–28]. In contrast, the pro-oxidant activity of CNPs sensitises pancreatic cancer to radiotherapy by producing ROS [28]. The presence of intracellular CNPs in normal, stromal,

and tumour cells also serve for anticancer therapy and reduces adverse effects [29]. It should be noted that under acidic tumour microenvironments, CNPs become inert [26], suggesting that they do not produce toxic ROS in tumour. In fact, it is still controversial whether the alternation between anti-oxidant and pro-oxidant activities of CNPs is driven merely by slight pH differences, i.e. in weakly acidic or neutral/weakly basic microenvironments [30]. That is, not only redox but also non-redox reactions of CNP may be involved in their therapeutic mechanism [30]. Indeed, our previous study has revealed that under a physiological pH, i.e. independently of pH, extracellular CNPs with dominant Ce^{3+} or Ce^{4+} ions inhibit or promote the growth of normal mesenchymal stem cells, respectively [31]. Additionally, at weakly basic pH, redox reactions of extracellular CNPs have been suspended due to phosphorous blocking at Ce^{3+} ion sites [31–34]. These insights also imply the potential that non-redox mechanisms of CNPs are working, but their mechanisms have yet to be fully elucidated. These emerging themes may be key to understanding the non-redox mechanisms of CNPs for anticancer treatment via direct and indirect cell-CNP contacts in tumour microenvironments.

Upon exposure to biofluids such as serum and plasma, which contain components of the ECM in normal and tumour microenvironments, the surface characteristics of NPs can undergo transformation due to the adsorption of proteins, resulting in a surrogate biological identity [35]. The adherence of proteins on the NP surface leads to the formation of "protein coronas," which have gained significant attention due to their ability to confer a bio-adaptive surface onto artificial NPs [35–38]. The composition and structure of protein corona are influenced by the physicochemical properties of NP surfaces and the biological components present in their surroundings [37]. Nanoparticles with a protein corona, e.g. including the epitope exposure [38], have the potential to engage in specific interactions, such as receptor-mediated cell-NP interaction.

Therefore, the specific proteins adsorbed onto these NPs, including CNPs, may be involved in the receptor-mediated interaction between cells and extracellular NPs. The effects of cell-CNP contact on tumour cell growth and the tumour-targeting capabilities of CNPs remain unknown. Since Ce valence state of extracellular CNPs greatly affects normal mesenchymal stem cells [31], this study focused on mesenchymal tumour cells, especially those induced by pEMT, as they provide maximum stemness relevant to malignant cancer stem cell-like features [1,2]. In solid tumours, including tumour microenvironments, cancer stem-like cells are crucial targets for chemotherapy to prevent cancer metastasis and therapeutic resistance [1,2]. Targeting pEMT states in cancer, thus, is valuable for therapeutic strategies aimed at pEMT-induced tumour cells, including cancer stem-like cells. Therefore, this study demonstrates the potential of extracellular CNPs to selectively inhibit the growth of pEMT-induced tumour cells without affecting uninduced epithelial tumour cells, and explores the possibility of pEMT-targeting anticancer treatments using the non-catalytic biointerface of CNPs with adsorbed proteins.

2. Experimental section

2.1 Fabrication: The fabrication of CNP-layered poly-L-lactic acid (PLLA) substrates (CNP/PLs) and their surface treatment to convert the dominant Ce^{4+} to dominant Ce^{3+} ions has been previously described [31,39]. Briefly, negatively charged CNPs with dominant Ce^{4+} ions were coated on PLLA surfaces (named, A-IV). The CNPs used were formed by a gas-phased reaction between metal and oxygen using physical vapour synthesis, and the chemical compositions of CNPs are shown in Table S1(CIK NanoTek Co., Tokyo, Japan). In addition, A-IV was irradiated by Ar ions at a radio-frequency bias power of 200 W for 60 s, resulting in positively charged CNP/PLs with highly concentrated Ce^{3+} ions (B-III) via charge compensation. The cross-sectional image of

typical CNP/PLs was observed by transmission electron microscopy (TEM), and the Ce 3d spectra of A-IV and B-III were detected by Xray photoelectron spectroscopy (XPS) with a monochromatic AlKa X-ray source (Theta Probe, Thermo Fisher Scientific K.K., Japan). The surface charge analysis of the CNPs was carried out on the A-IV and B-III surfaces using a zeta potential analyser with a plate attachment (ELSZ-1000, Otsuka electronics Co., Ltd., Osaka, Japan). The detailed characteristics of A-IV and B-III were evaluated in our previous reports [31,39].

2.2. Cell culture and EMT induction: Human non-small cell lung cancer cell line A549 cells were incubated with Dulbecco's modified Eagle medium (low-glucose) supplemented with 10% foetal bovine serum (FBS) and 1% penicillin-streptomycin (PS). Before cell seeding on samples, A549 cells were cultured in tissue culture (TC) flasks for 72 h. A549 cells show epithelial morphology and collective migration. EMT has been known to be induced in tumour cells by several external stimuli, such as transforming growth factor β (TGF-β), epidermal growth factor, and fibroblast growth factor [40]. Collagen type-I (Col-I) has also been confirmed to readily induce EMT in lung adenocarcinomas and pancreatic and breast cancer cells [41,42]. TGF-β is the most potent EMT initiator; however, it acts as a tumour suppressor during the early disease period, whereas its actions on tumour cells and their microenvironment promote cancer progression at a later stage [2]. In this study, to avoid the biphasic effects of TGF-β, EMT was induced using Col-I. Since EMT in A549 cells can be induced by incubating on Col-I for 48 h [42], cells were cultured on Col-I dishes (AGC Techno Glass Co., LTD, Shizuoka, Japan) for at least 72 h (Col-I/A549). During this period, most of the cells had already adopted a fibroblast-like morphology and exhibited independent migration, consistent with previous reports of EMT-induced tumour cells treated with TGF-β or cultured on Col-I [41–43]. It should be noted that EMT induced by Col-I was partial compared to that induced by TGF-β (the characteristics of EMT induced by Col-I and

TGF-β will be described later). Cells were seeded onto UV-sterilised CNP/PLs (A-IV and B-III), PLs, Col-I, and TC, at a density of 0.5 or 1×10^4 cells/cm^2. All cell cultures were maintained in an incubator equilibrated with 5% CO_2 at 37 °C.

2.3. Cytotoxicity of possibly dissolved cerium ions: To assess the cytotoxicity of potentially dissolved cerium ions released from CNP/PLs, samples (PL, A-IV, and B-III: 10 × 10 mm; $S = 1.0$ cm^2) were immersed in culture media (250 μL, half the quantity used when culturing in 24-well TC plates) and incubated for 24 and 72 h in an incubator with 5% CO_2 at 37 °C. A549 or Col-I/A549-C3 (pre-cultured on Col-I for 3d) cells were seeded into a 96-well TC plate, with 50 μL of fresh media (1×10^3 cells/well). After pre-incubation for 1 h, the supernatant that had been immersed with samples for 24 and 72 h was transferred into the 96-well plates with cells (50 μL/well). Cytotoxicity was assessed 24 h after incubation using the Cell Counting Kit-8 (CCK-8, DOJINDO LAB., Kumamoto, Japan). Absorbance of the supernatant with cells at 450 nm and 650 nm wavelengths was measured using a microplate reader. The assay was performed according to the manufacturer's instructions.

2.4. Cell adhesion assay: For the cell adhesion assay on PL, A-IV, and B-III (10 × 10 mm; $S = 1.0$ cm^2), A549 or Col-I/A549-C3 cells were seeded into 24-well TC plates with samples, at 5×10^4 cells/cm^2. After culturing for 3 h, the samples were washed with phosphate buffered saline (PBS), and then transferred to another 24-well TC plates with fresh media containing the CCK-8 reagent. After incubation for 1 h, 100 μL of the supernatant was transferred into a 96 well plate, and the absorbance of the supernatant at 450 nm was measured using a microplate reader.

2.5. Cell adhesion/proliferation/viability assay: To retain a mesenchymal phenotype in A549 cells for an extended period, Col-I/A549-C5 (pre-cultured on Col-I for 3 days and then 2 more

days, totalling 5 days) cells were used for cell adhesion (at 24 h), cell proliferation, and cell viability assays (up to 72 h). A549 and Col-I/A549-C5 cells were cultured on PLs, CNP/PLs (10 × 10 mm; S = 1.0 cm^2), and Col-I cover glass (ϕ12 mm; S = 1.1 cm^2; AGC) in an ultra-low adhesive 24-well plate (Low-Ad). TC surface (S = 1.9 cm^2) was used as a control. After 24, 48, and 72 h of cell culture, the CCK-8 reagent was added into the 24-well plates. After incubation with CCK-8 reagent, the assay was performed as described in 2.4.

2.6. Cell alive/death assay: Cells were stained with calcein AM and propidium iodide (PI) using the Cellstain® Double Staining Kit (CS01, DOJINDO), and subsequently observed using an inverted fluorescence microscope (ZOE cell imager, Bio-Rad Laboratories, Inc., CA, USA) with filters at λ = 490 nm and 545 nm.

2.7. Immunocytochemistry: In brief, cells were fixed with 4% paraformaldehyde and treated with 0.1% Triton X-100. After blocking with 1% bovine serum albumin (BSA)/PBS, the cells were incubated with a primary antibody: anti-N-cadherin (bs-1172R, Bioss Inc.,) or anti-Ki-67 [SP6] (ab16667, Abcam, Cambridge, UK) in 1% BSA/PBS at 4 ℃ overnight. The goat anti-rabbit IgG H&L with Alexa Fluor® 488 (ab150077, Abcam) was used as the secondary antibody. F-actin and nuclei were stained with phalloidin-iFluor 594 (ab176757; Abcam) and DAPI. Cells treated with SlowFade™ (S36967, Thermo Fisher Scientific K.K., MA, USA) were observed using a confocal microscope (TCS SP5, Leica Microsystems, Wetzlar, Germany).

2.8. Quantitative real time polymerase chain reaction (qRT-PCR): Total RNA was extracted using Isogen (311-02501, Nippon Gene Co., Ltd., Tokyo, Japan), treated with DNase I and RNase inhibitors (2270A and 2313A, Takara, Shiga, Japan), and purified using Agencourt RNAClean XP (A63987, Beckman Coulter, Inc., CA, USA), according to the manufacturer's instructions. RNA

was quantified using a visible spectrophotometre (NanoDrop, Thermo). RNA was reverse-transcribed into cDNA using a PrimeScript™ RT reagent kit (RR037A, Takara). Quantitative real-time PCR was performed using LightCycler® 480 SYBR Green I Master (04707516001, Roche, Basel, Switzerland) in a real-time PCR system (LightCycler 480SystemII, Roche). Primer sequences used are as follows,

GAPDH-F; GGAGCGAGATCCCTCCAAAAT, GAPDH-R; GGCTGTTGTCATACTTCTCATGG, E-cad-F; GGATAGAGAACGCATTGCCACATAC, and E-cad-R; CCATTGGATCCTCAACTGCATTCC.

2.9. Western blot analysis: Briefly, cells were lysed in a blue-lading buffer pack (#7722, Cell Signaling Technology, Inc., MA, USA) with a protease inhibitor (87786, Thermo) and a phosphatase inhibitor (P5726, Sigma-Aldrich, MO, USA). The total protein was quantified using a NanoOrange™ protein quantitation kit assay (N6666, Thermo). Cell lysates were routinely separated on polyacrylamide electrophoresis gels, and western blot analysis was performed using iBlot Gel Transfer Stacks Gel (PVDF, Invitrogen, MA, USA). Nitrocellulose membranes were blocked in 5% BSA/TBST for 1 h at room temperature. Primary antibodies against E-cadherin (#3195), Ki-67 (ab16667) focal-adhesion kinase; FAK (#13009), phosphorylated focal-adhesion kinase; pFAK-Y397 (#3283), and GAPDH (ab9485) were purchased by CST or Abcam. Membranes were incubated with primary antibodies diluted in 5% BSA/TBST overnight at 4 ℃, and then with horseradish peroxidase (HRP)-linked secondary antibodies (#7074, CST) in 5% skim milk/TBST for 1 h at room temperature. Chemiluminescence analysis was performed using immobilon western chemiluminescent HRP substrate (WBKLS0100, Millipore). Densitometric measurements of band intensities were performed using the ImageJ software.

2.10. Protein adsorption assay: For direct coating process, samples (PL, A-IV, and B-III: 4 × 4 mm) were fixed on a PDMS-coated culture dish to prevent protein adhesion to their backsides, and then immersed in protein solutions containing fibronectin (FN; 063-05591, Wako, Japan), laminin (LN; 120-05751, Wako), and serum-based culture medium (E-MEM with 10% FBS and 1% PS). Instructions for protein coating were derived from relevant instruction manuals. The concentrations used were 5 μg/cm^2 for FN and LN coating, based on the recommended levels in each manual. The samples were incubated in a CO_2-gas incubator at 37 °C for 30 min. For the electrophoresis assay, detailed conditions of serum-derived protein corona on respective materials and the observation of SDS-PAGE gel have been previously described [31,39]. The densitometry of the total protein corona in SDS-PAGE gel were analysed using Image J software.

For immunofluorescence analysis, samples (PL, A-IV, and B-III: 4 × 4 mm) were washed twice in PBS and then immersed in 4% paraformaldehyde and 0.5% Triton X-100. The sample surfaces were blocked with 1% BSA solution for 30 min, followed by incubation with the primary antibodies anti-FN (ab2413) and anti-laminin (ab11575) and with the secondary antibody goat anti-rabbit IgG H&L with Alexa Fluor® 488 (ab150077) for 1 h at room temperature. Fluorescence from the samples in a 96-well black plate with hydrophilic treatment was measured using a fluorescence microplate reader (λ_{EX} / λ_{EM} = 485 nm / 530 nm).

2.11. Intracellular ROS Assay: The pEMT/A549 cells were cultured on TC, A-IV and B-III (4 × 4 mm) in a 96-well black bottom clear TC plate for 72 h. The generation of intercellular ROS was compared using ROS assay kit (R253, DOJINDO) with photo-oxidation resistant dichlorofluorescindiacetate (DCFH-DA). Untreated cells on TC in Hanks Balanced Salt Solution (HBSS, Thermo) were used as negative controls, while treated cells on TC with 500 μM-H_2O_2 in

HBSS were used as positive controls. Dye fluorescence from cells on sample in HBSS was detected by a fluorescence microplate reader (λ_{EX} / λ_{EM} = 490 nm / 530 nm). Measurements were taken at 15 min intervals up to 60 min. The data collected were the average value of 9 multi-points on the sample surfaces with 1 mm intervals.

3. Results

3.1. Cytotoxicity of possibly dissolved cerium ions and tumour cell adhesion

Typical CNPs are hardly dissolved in culture media, but the CNP/PLs used in this study, with a particle diameter of 2–3 nm (on CNP/PLs, **Fig. 1a**) and highly concentrated Ce valent states (about 75 atm%-Ce^{4+} and -Ce^{3+} ions; A-IV and B-III, **Fig. 1b** and **Table S2**), may release minimal amounts of soluble cerium ions, potentially influencing cytotoxicity. High-density cell adhesion assays (close to a confluent state, **Fig. S1a**) revealed that, for A549 cells, the cell morphologies appeared similar (**Fig. S2**), and different substrate materials did not show statistically significant differences in tumour cell adhesion (the upper panel in **Fig. 2a**). For A549 cells pretreated on Col-I for 3 days (hereafter, Col-I/A549-C3), although A-IV decreased cell adhesion compared with TC and PL, there was no significant difference between A-IV and B-III (the lower panel in Fig. 2a), indicating that the effects of Ce valence states of CNP/PLs on tumour cell adhesion were minimal. Furthermore, to assess the cytotoxicity of the supernatant immersed with CNP/PLs, A549 and Col-I/A549-C3 cells were cultured under the conditions shown in **Fig. S1b**. Regardless of the substrate materials (TC, PL, A-IV, and B-III) and the immersion time in serum-based culture media (24 and 72 h), the cell viabilities of both A549 and A549/Col-I-C3 cells remained unchanged (**Fig. 2b**). Thus, the cytotoxicity of cerium ions potentially dissolved from A-IV and B-III states was negligibly low. In addition, considering the formation of the protein corona on NPs in a serum-based culture medium, the modified medium itself, due to the reduction of serum components and quantities, may potentially cause cytotoxicity [35]. The culture media immersed with CNP/PLs, however, did not exhibit cytotoxicity (Fig. 2b).

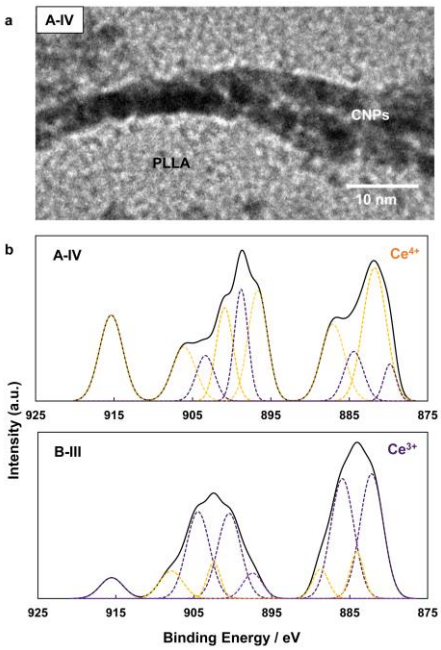

Fig. 1. Characteristics of typical CNP/PLs. a. A TEM image of typical CNP/PL cross-section, and **b.** XPS Ce3d spectra of A-IV and B-III.

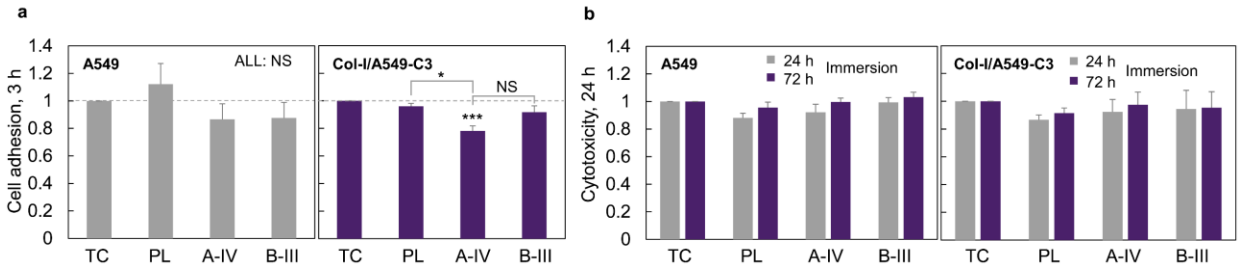

Fig. 2. High-dense cell adhesive assay and cytotoxicity assay in supernatants with metal ions possibly released from materials., **a.** cell adhesion of A549 and Col-I/A549-C3 cells to each material under the high-density condition at 5×10^4 cells/cm^2 (NS, not significant; *, $p < 0.05$; ***, $p < 0.005$), and **b.** cytotoxicity of culture media immersed with TC, PL, A-IV, and B-III for 24 and 72 h. Bars are representative of three independent experiments.

3.2. Partial EMT-induction

Uninduced A549 cells showed collective migration and cell-cell adhesion, indicative of an epithelial phenotype (**Fig. 3a**). In contrast, Col-I-treated A549 cells acquired a fibroblast-like morphology and individual migration, indicating that EMT was initiated. Col-I/A549 cells exhibited downregulated mRNA expression levels of E-cadherin (E-cad, a specific EMT marker), but they remained about 40% of those observed in A549 cells (**Fig. 3b**). According to the western blot analysis in Fig. 3b, TGF-β treatment resulted in a complete loss of E-cad protein expression (full EMT). By contrast, though Col-I treatment drastically reduced E-cad protein levels, Col-I/A549-C5 cells (pretreated for 5 days on Col-I) remained at approximately 1/3 of those observed in A549 cells. These findings indicate that Col-I treatment induces partial EMT (pEMT), rather than full EMT, in A549 cells. Therefore, Col-I/A549-C5 cells were used as pEMT/A549 cells hereafter.

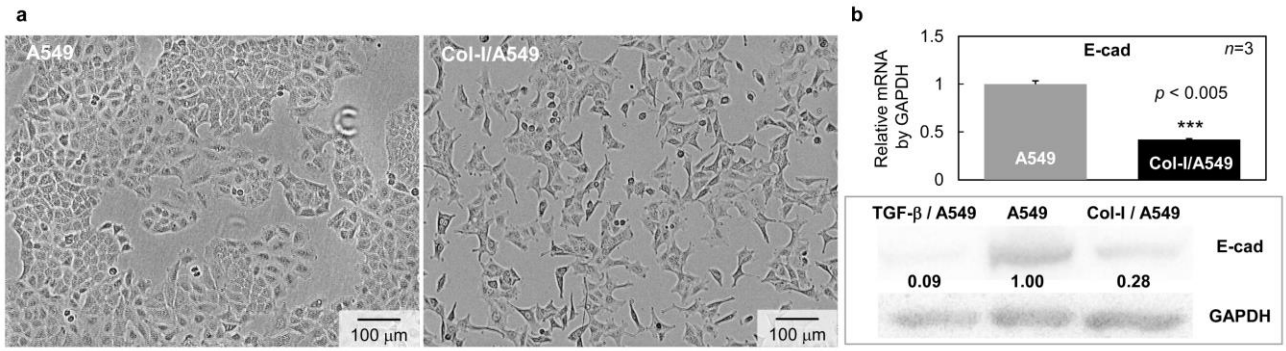

Fig. 3. Characteristics of A549 and Col-I/A549 cells for induction of pEMT. a. Typical cell morphology of A549 and Col-I/A549-C3. **b.** The mRNA levels of E-cad genes in A549 and Col-I/A549 determined by qRT-PCR, and the western blot analysis of E-cad expression in A549 (uninduced EMT), Col-I/A549-C5 (partial EMT), and TGFβ-derived A549 (full EMT) cells.

3.3. Selective inhibition of pEMT/A549 cell growth

Most pEMT/A549 cells on A-IV and B-III at 48 h retained a round shape or exhibited limited cell spreading compared with pEMT/A549 cells on TC (**Fig. 4a**), suggesting that CNP/PLs inhibit the growth of pEMT/A549 cells. To confirm the selective inhibition of pEMT/A549 cell growth on CNP/PLs, the cell adhesion, proliferation, and viability of A549 and pEMT/A549 cells on each material were compared (Fig. 4b). As expected, uninduced epithelial A549 cells similarly proliferated on A-IV and B-III as well as TC and PL. The adhesion of A549 cells to TC and PL at 24 h after seeding, as well as their proliferation and viability up to 72 h, showed no statistically significant differences (the upper panels in Fig. 4b), indicating that neither A-IV nor B-III had an impact on epithelial tumour cells. Nevertheless, in the case of pEMT/A549 cells (the lower panels in Fig. 4b), though B-III slightly decreased cell adhesion at 24 h, both A-IV and B-III significantly delayed proliferation at 72 h and drastically reduced cell viability at 72 h. Interestingly, B-III had been already initiated the reduction of cell viability at 24 h. As a result, B-III reduced cell viability to 58% of that on TC at 72 h (c.f. A-IV decreased it to 71% of that on TC at 72 h). These findings provide evidence that extracellular CNPs have the capability to selectively inhibit the growth of pEMT-induced tumour cells.

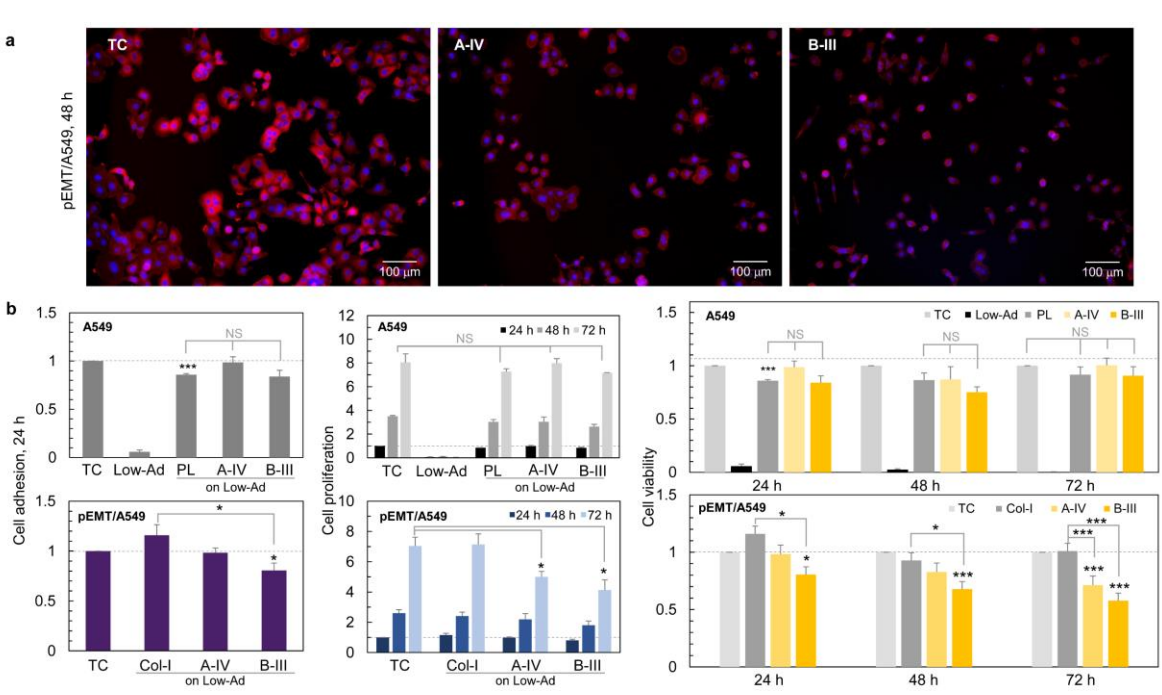

Fig. 4. Selective inhibition of pEMT/A549 cell growth on A-IV and B-III at 24, 48, and 72 h. **a.** Cell morphologies, **b.** cell adhesion, proliferation, and viability of A549 (upper panels) and pEMT/A549 (lower panels) cells on A-IV and B-III, as well as TC, PL, Low-Ad, or Col-I plates. Both A-IV and B-III selectively reduced the proliferation and viability of pEMT/A549 cells (n = 3; NS, not significant; *, $p < 0.05$; **, $p < 0.01$; ***, $p < 0.005$).

3.4. Retaining mesenchymal phenotype

Upregulated N-cadherin (N-cad) expression in cells is indicative of the mesenchymal phenotype. To determine whether the mesenchymal phenotype was retained in pEMT/A549 cells on CNP/PLs, N-cad expression in cells on PL, A-IV, and B-III were compared using immunocytochemistry. Even at 72 h, a high expression of N-cad was observed in pEMT/A549 cells on A-IV and B-III (**Fig. S3**), indicating that CNP/PLs possess the capability to retain the mesenchymal phenotype. (c.f. low expression levels of N-cad in pEMT/A549 cells on PLs, suggesting a mesenchymal-to-epithelial transition (MET)). Thus, the MET-mediated re-epithelial tumour cells on PL could

accelerate cell growth, whereas the pEMT-retained tumour cells on CNP/PLs may experience growth delay.

3.5. Non-induction of apoptosis and ROS generation

CNPs taken up into tumour cells potentially induce apoptosis due to the production of toxic ROS via the redox cycle between Ce^{4+} and Ce^{3+} ions of CNPs in an acidic environment [44–46]. To assess this, a cell alive/death assay was performed on TC, negatively charged A-IV, and positively charged B-III. However, late-phase apoptosis was barely observed regardless of the surface charges and Ce valence states of the CNPs (**Fig. S4a**). Additionally, the ROS generation on TC, A-IV, and B-III did not show statistically differences (**Fig. S4b**). These results indicate that the mechanisms through which extracellular CNPs in CNP/PLs selectively inhibit pEMT-induced tumour cell growth are not associated with apoptosis and redox-related ROS generation. In fact, the effect of redox-related ROS production by CNPs in the environments of pEMT-induced tumour cells (i.e. at a physiological pH in culture media) is negligibly low or unrelated to the inhibition of growth. Therefore, extracellular CNPs under the physiological pH environment act as a cytostatic agent for pEMT-indued tumour cells rather than an inducer of apoptosis. At physiological pH, since phosphorus blockings at Ce^{3+} sites are known to suspend redox-related pro-oxidant activity, e.g. SOD mimicking activity [32–34], the non-redox mechanism of extracellular CNPs in the environments of pEMT-induced tumour cells could be highly related to the inhibition of cell growth.

3.6. Cell cycle arrest at G0 phase

The most recognised characteristic of tumour cells, in general, is their abnormally rapid growth with uncontrolled cellular division. However, the selective inhibition of pEMT/A549 cell growth

on CNP/PLs (Fig. 4) suggests that extracellular CNPs may delay the division of tumour cells via cell cycle arrest. To evaluate cell cycle arrest in pEMT/A549 cells on PLs and CNP/PLs, immunocytochemistry using Ki-67 antibodies was performed (**Fig. 5a**). Ki-67 expression in nuclei represents cell cycle progression at the G1, S, G2, and M phases, whereas absence of Ki-67 expression indicates cell cycle arrest at the G0 phase. Most of the pEMT/A549 cells on PL showed high expression of Ki-67, indicating cell cycle progression at the G1, S, G2, and M phases. As a result, these cells on the PL rapidly proliferated and reached a confluent state. However, pEMT/A549 cells on A-IV and B-III exhibited negative or significantly low expression of Ki-67 (dotted circles in Fig. 5a). Based on the counting assay of Ki-67-negative nuclei and immunoblotting analysis of Ki-67 (**Fig. 5b**), the order of negative Ki-67 expression was PL < A-IV < B-III, which resembled the order of pEMT/A549 cell growth inhibition: TC ≈ Col-I < A-IV < B-III (the lowest panel in Fig. 4b). Indeed, A-IV and B-III induced cell cycle arrest at the G0 phase in pEMT-induced tumour cells, indicating that depending on Ce valence states of CNP/PLs, extracellular CNPs promote the transition from cytostatic phases to the quiescent-like G0 phase. Noted that cell cycle arrest is divided into two stages: permanent/irreversible cell arrest (i.e. senescence) and temporal/reversible cell arrest (i.e. quiescence/dormancy). Senescent cells acquire a flatten/enlarged morphology and cytoplasmic vacuolisation [47]. However, these senescence-specific properties were not observed in Ki-67-negative pEMT/A549 cells (Fig. 5), suggesting that the cell cycle arrest at the G0 phase on CNP/PLs represents not senescence but quiescence/dormancy.

Under stresses such as serum starvation and ROS production, some cells potentially arrest cell cycle at different phases [48–50]. However, the present study was carried out under sufficient serum-based environments. The variation of ROS production levels in cells on A-IV, B-III and TC

did not show (Fig. S4b). Thus, the induction of quiescence/dormancy in pEMT/A549 cells is not due to the cell cycle arrest caused by these stresses.

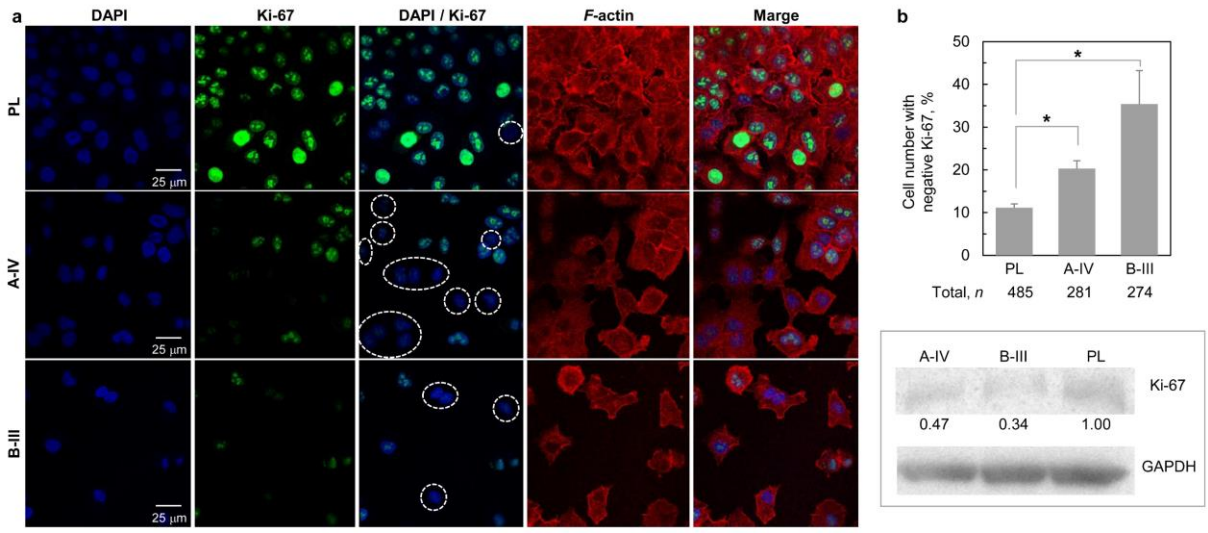

Fig. 5. Ki-67 expression in pEMT/A549 cells cultured on PLs, A-IV, and B-III at 72 h. a. Immunofluorescence analysis of Ki-67 (Ki-67, green; nuclei, blue; F-actin, red). b. Ratio of Ki-67-negative cell number (*, $p < 0.05$), and immunoblotting analysis of Ki-67 and GAPDH. The majority of cells on PL were Ki-67-positive, indicating cell cycle progression at the G1, S, G2, and M phases. By contrast, most of the cells on A-IV and B-III were Ki-67-negative, indicating cell cycle arrest at the G0 phase. Both the cell counting and immunoblotting assays provided consistent results, showing the same order of Ki-67-negative phenotype: PL < A-IV < B-III. This suggests that depending on the Ce valence states, extracellular CNPs promote the transition from cytostatic phases to the quiescent G0 phase.

3.7. Protein adsorption

The physicochemical properties of NPs potentially influence the adsorption states of proteins in the protein corona, such as components, steric hindrance/epitope-hidings, and soft/hard structures [35–38]. Similarly, Ce valence states may impact the characteristics of CNP-specific protein corona. After exposure to serum-based media, although the total amounts of proteins adsorbed on CNPs/PLs are independent on Ce valent states [31], their SDS-PAGE analysis provides different band profiles in response to Ce valent states [31]. Based on quantitative one-dimensional profiles of serum-derived protein coronas on materials, distinct components with different molecular weights were observed on PL, A-IV, and B-III (**Fig. 6a**). The surface features of CNPs such as Ce valence states may relevant to determining specific components and conformational changes of adsorbed proteins.

In solid tumours, various ECM proteins such as fibronectin (FN), laminins (LN), and collagens (Col) are highly expressed [17,51–53]. To demonstrate the difference in protein adsorption on respective materials, the amounts of FN/LN adsorption were evaluated under two conditions: *non-specific* adsorption by *direct* protein coatings; and *competitive and specific* adsorption by immersion into serum-based culture media. Though the *direct and non-specific* adsorption of FN/LN on different materials showed no statistically significant differences, their *competitive and specific* adsorption increased the amounts of FN/LN adsorption on A-IV compared with those on PL and B-III (**Fig. 6b**). This suggests that Ce valence states contribute to determining protein corona components on CNP surfaces. The low amounts of FN/LN on A-IV (i.e. no peaks of FN; 210-250 and LN; 220/205 kDa in Fig. 6a) imply a weak interaction between cells and FN/LN, but other ECM-derived cell-adhesive proteins, such as vitronectin and Col, which are similar to FN/LN, may readily adsorb to A-IV, leading to the formation of CNP-specific

protein corona on A-IV. The physicochemical properties of NPs affect the features of protein corona such as components, conformation, steric hindrance/epitope-hidings, soft/hard layered structures, and cell-membrane/protein interaction [35–38]. Thus, different Ce valence states may also influence the adsorption states of CNP-specific proteins (e.g. direction of protein adsorption, their conformational change, and steric barrier), resulting in the formation of stereo-specific protein corona.

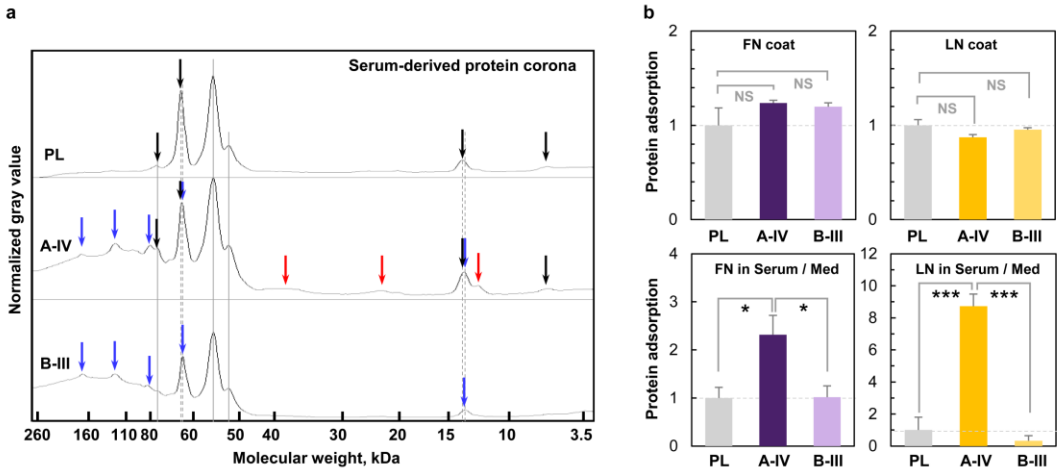

Fig. 6. One-dimensional profiles of protein coronas and densitometry of non-specific/specific adsorption of FN/LN on PL, A-IV, and B-III. a. Profiles of protein coronas formed on the materials immersed in serum-based culture media (arrows: black, common to PL and A-IV; red, A-IV original; and blue, common to A-IV and B-III). **b.** Non-specific adsorption of FN and LN after their direct coatings, and specific adsorption of FN and LN on materials exposed to serum-based media ($n = 3$; NS, not significant; *, $p < 0.05$; ***, $p < 0.005$).

3.8. Suppression of phosphorylated focal-adhesion kinase (pFAK)

Cell-ECM contacts directly cause drug resistance of tumour via an integrin and focal-adhesion kinase (FAK) signaling [17]. Given that ECM-derived proteins adhered on CNPs act as ligands to stimulate or prevent receptor-mediated cell-NP interactions (e.g. integrin receptors), the downstream signalling of integrin receptors could influence pFAK/FAK-related cell functions, such as cell viability and growth. FAK, a mediator in integrin-associated cell adhesions, plays a critical role in growth-factor signalling, cell proliferation, survival, and migration [54]. In particular, FAK serves as a regulator for cell intrinsic signals promoting proliferation [54,55]. The mechanism of FAK activation involves the clustering of integrin receptors when cells bind to adhesive proteins in the ECM [55–57]. Following integrin activation mediated by cell-ECM interactions, FAK is autophosphorylated at Tyr397 (pFAK-Y397), which then recruits members of the Src-family kinases, resulting in phosphorylation of FAK at other Src-specific tyrosine phosphorylation sites (e.g. Y861, Y567/577, and Y925) and activation of Erk and Akt [58]. Thus, FAK activation triggered by pFAK-Y397 promotes cellular viability and proliferation. Conversely, inhibiting FAK can reduce tumour cell viability and growth [59]. Given that CNP/PLs with serum/ECM-derived proteins can downregulate pFAK-Y397 expression via integrin-associated adhesions in pEMT-induced tumour cells (i.e. given that extracellular CNPs with specific proteins act as pFAK-Y397 inhibitors, similar to integrin antagonists), the viability, growth, and proliferation of pEMT/A549 cells would be decreased. To confirm this, the ratio of pFAK/FAK expression in cells on TC, Col-I, TC, A-IV and B-III were evaluated by immunoblot analysis. As expected, both A-IV and B-III enabled the reduction of pFAK-Y397 expression in pEMT/A549 cells, with B-III showing a more pronounced decrease (**Fig. 7a**). The pFAK-Y397/total-FAK ratios on A-IV and B-III were reduced to 72% and 45% compared with Col-I, respectively (**Fig. 7b**).

These reductions resembled those of the cell viability at 72 h (71% on A-IV and 58% on B-III; the lowest panel in Fig. 4b). The components or structures of proteins adsorbed on CNPs in response to Ce valance states may relevant to pFAK expressions. Thus, the receptor-mediated cell interaction with CNP-specific proteins may contribute to the pFAK/FAK-associated growth inhibition of pEMT/A549 cells on CNP/PLs.

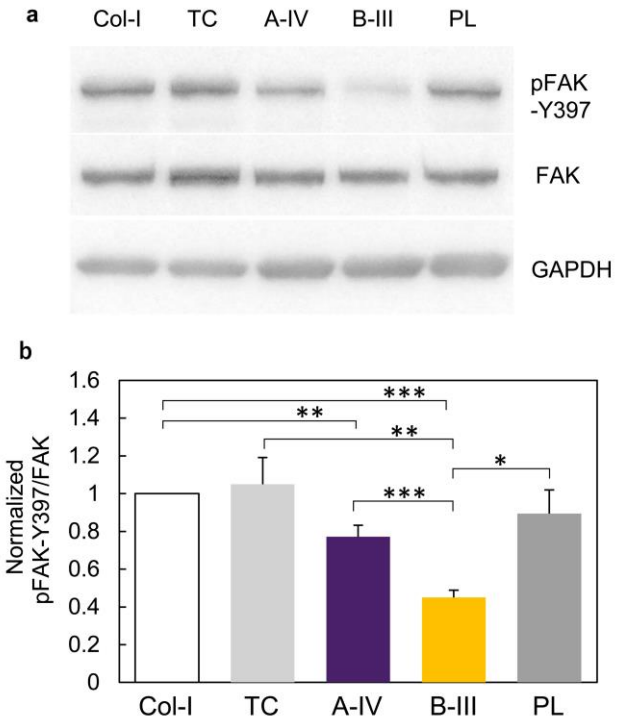

Fig. 7. Effect of Ce valence state in extracellular CNPs on pFAK-Y397 expression. a. Western blot analysis of pFAK-Y397, FAK, and GAPDH expression in pEMT/A549 cells on Col-I, TC, PL, A-IV, and B-III. **b.** Densitometry of the western blot bands. The bar chart represents densitometric readings relative to protein levels on Col-I. $n = 4$ independent experiments (*, $p < 0.05$; **, $p < 0.01$; ***, $p < 0.005$).

4. Discussion

The dynamic induction of EMT in cancer contributes to various features, such as tumour stemness, therapeutic resistance and adaptation to the altered tumour microenvironment, linking them to cancer stem cell-like features [2]. Furthermore, therapeutic interventions, such as chemotherapy and irradiation therapy, often promote EMT/pEMT [2], which is linked to the acquisition of multidrug resistance. The emergence of EMT/pEMT-induced mesenchymal tumour cells is frequently associated with a poor prognosis in cancer patients [1,60]. Therefore, targeting EMT/pEMT in cancer has the potential to improve the therapeutic sensitivity of chemoresistant tumour cells. For instance, several methods have been developed that employ molecules to block or reverse the EMT state [2] by utilising miRNA to interfere with EMT transcription factors [61–63]. These EMT-blocking and reversing approaches can retain the epithelial phenotype or promote re-epithelialisation (i.e. MET), resulting in highly proliferative epithelial tumour cells. In addition, these approaches enable tumour cells to regain therapeutic sensitivity against standard anticancer drugs that target proliferative cells. However, they may also increase the risk of tumour regrowth and cancer metastasis. Furthermore, since EMT modulates normal tissue homeostasis and wound healing, careful evaluation is necessary to assess the potential adverse effects of EMT-blocking or reversing agents. In contrast, trapping proliferative cancer cells in a permanent growth-arrested or cytostatic state without inducing cell death pathways has shown promising results in preliminary clinical investigations [64,65]. Therefore, this study aimed to effectively trap proliferative tumour cells in a growth-arrested or cytostatic state without inducing apoptosis, and examined whether extracellular CNPs selectively inhibited the growth of pEMT-induced tumour cells without affecting epithelial tumour cells. The present study revealed that extracellular CNPs selectively trapped pEMT-induced tumour cells in a growth-arrested quiescent/dormant or cytostatic state

without inducing apoptosis. In addition, extracellular CNPs selectively inhibited the growth of pEMT-induced tumour cells with a hybrid epithelial / mesenchymal phenotype, without influencing full epithelial tumour cells. Importantly, neither redox-related ROS generation nor inducing apoptosis by CNPs was linked to the growth inhibition of pEMT-induced tumour cells, indicating that the non-redox mechanisms of extracellular CNPs was associated with this tumour cell growth inhibition. When dominant Ce^{3+} ions are present on extracellular CNPs, *highly efficient* selective growth inhibition of pEMT-induced tumour cells occurs; however, full epithelial tumour cells are not affected. Dominant Ce^{4+} ions on extracellular CNPs are known to induce the growth of normal mesenchymal stem cells [31]; however, they successfully inhibited the growth of pEMT-induced tumour cells in this study. That is, when dominant Ce^{4+} ions were present, there was *high selectivity* between the regulation of normal mesenchymal and tumour epithelial/mesenchymal cell growth, leading to fewer adverse effects. These findings provide the first evidence that pEMT-induced tumour cells' growth is selectively inhibited by extracellular CNPs with dominant Ce^{3+} and Ce^{4+} states.

Precise targeting of NPs, which reduces side effects and drug resistance, has benefits in cancer treatment [66–68]. Currently, NPs used as drug delivery nanocarriers have been achieved using various materials, including lipid-based (e.g. liposomes, protein or cell membrane), polymeric and inorganic (e.g. metal, metal-oxide or quantum-dot) materials [8,9]. Physicochemical properties, such as size, shape and surface charge, are essential factors in determining the accumulation efficiency of NPs in tumours by the EPR effect. For instance, the adjustable sizes of NPs provide advantages to escape their capture by macrophages in the immune system and prevent their rapid leakage into blood capillaries [69]. Smaller NPs of <10 nm can be rapidly eliminated by the kidneys, as the threshold size for renal clearance is 5–6 nm, leading to a short lifespan in circulation.

In contrast, larger NPs of >200 nm induce poor tumour extravasation and risk activating the complement system [70]. Therefore, NP sizes of about 100 nm (<200 nm [69,71,72] or 50–150 nm [10]) have been identified to achieve passive targeting of tumours through the EPR effect [8,15]. In addition, a recent study has demonstrated that NPs with sizes of 12 nm exhibit tumour targeting with minimum to no nonspecific uptakes, while larger-sized NPs of 13 nm accumulate highly in major organs, such as the lungs, liver and pancreas [73]. This emphasises the importance of the size control of NPs, even by a few nm. When compared with sphere-shaped NPs, non-sphere-shaped NPs, such as rods and filaments, have been shown to readily accumulate in the spleen, lungs and especially in tumours [74–76]. This is due to the restricted uptake by macrophages or delayed clearance by the mononuclear phagocytic system [74–76], leading to a longer circulating lifetime [77,78]. Highly positive charges allow NPs to be detained by the vascular endothelial luminal with numerous negatively charged phospholipids, while highly negative charges induce the clearance of NPs by the liver, spleen or other parts of the reticuloendothelial system [10,79]. Therefore, the optimal physicochemical features of NPs for tumour accumulation by the EPR effect may be hydrodynamic diameters of 10–100 nm, a rod shape and a near-neutral charge or inorganic material composition [8,15]. Similarly, the physicochemical features of the CNPs investigated in the present study may be associated with tumour accumulation by the EPR effect. It should be noted that NPs have been described as having the potential to induce conformational changes in adsorbed proteins, and their resultant functionality could be exploited for therapeutic approaches to prevent cancer progression or improve tissue regeneration [80]. In this context, a small change of a few nm in the size of CNPs may play an important role in the conformational changes of the adsorbing proteins and their protein corona structures. In addition, since the stability of the Ce valence state is dependent on

the nanocrystal size, shape and facets [31,34,39], these factors may also strongly impact Ce valence-specific protein adsorption. Therefore, the morphological factors of the CNPs used (2–3 nm and spherical-like shape) may be vital for regulating Ce valence-specific proteins and their protein corona structures, which may correlate with the selective growth inhibition of pEMT-induced tumour cells. Accordingly, acquiring passive tumour-tissue targeting ability by the EPR effect may make it desirable to utilise the CNPs (2–3 nm and spherical-like shape) for surface functionalisation of optimally designed nanocarriers with, for example, a size between 10–100 nm and a rod shape.

The functionality of NPs with a serum or ECM-derived protein corona generally supports the specific recognition of cell surface receptors. When serum or ECM-derived cell-adhesive proteins non-specifically adsorb onto typical materials, integrin-mediated cell-material interaction can promote pFAK/FAK activation, leading to cell proliferation (on TC and PL, **Fig. 8a**). However, protein coronas on NPs are known to reduce nonspecific cell-NP interactions [37,81] and provide the potential for specific cell-NP interactions, such as receptor-mediated membrane adhesion, during cell association [37]. Likewise, CNP-specific protein coronas, including FN and LN, may induce intrinsic interactions, such as integrin-mediated cell-NP interactions, leading to the inhibition of pFAK/FAK-derived cell proliferation and the cell cycle arrest at G0 phase, i.e. quiescence/dormancy (**Fig. 8b**). For instance, highly expressed FN-1, LN and Col-I/IV in tumour cells and microenvironments are involved in cell quiescence [82,83]. In addition, Col17A1 in hemidesmosomes has been associated with the maintenance of cancer cell dormancy [84]. However, cell-NP interactions mediated by rare corona proteins are not currently well understood [57]. Furthermore, CNP-specific adsorbed proteins and their corona, along with their conformational changes and their composed stereo-specific protein corona, may act as ligands to

regulate quiescence/dormancy in pEMT-induced tumour cells. Assuming that CNP-specific protein coronas, such as those including FN and LN, regulate the quiescence/dormancy of pEMT-induced tumour cells on CNP/PLs, the receptor-mediated cell-CNP interactions could be involved. For instance, integrin-mediated cell interactions are well known to trigger pFAK/FAK activation relevant to FAK-mediated cell viability and proliferation [57,85]. The possibility that CNP-specific protein coronas interact with the integrin receptors of pEMT-induced tumour cells may explain the reasons for quiescence/dormancy and pFAK suppression in the cells attached to CNP/PLs, which can lead to a cytostatic state even without apoptosis. That is, the integrin-mediated cell-CNP contacts appear to interrupt the integrin and FAK-related signalling that promotes cell viability and proliferation.

Understanding the structure and conformational changes of adsorbed proteins on NPs has significant implications for modulating cell behaviour and providing insights into cancer treatments [80]. The formation of a protein corona consisting of adsorbed proteins and its responses to the physicochemical features of NPs and the bioenvironments are known to affect the therapeutic and pathophysiological effects of NPs [80,86,87]. In fact, the combination of a NP's physicochemical feature and its exposure condition, such as pH, temperature, ionic strength and protein concentration, can play a vital role in the determination of the adsorbed proteins' properties (e.g. density and conformational changes) and the protein corona's structure (soft or hard), resulting in the NP's unique functionality. The resultant NPs with a protein corona may be therapeutically efficient in preventing cancer growth. However, the optimal combination remains unclear due to the significant complexity of the correlations among these factors. For instance, FN adsorption increases on a hydrophobic surface of materials [88], whereas decreases on a hydrophilic surface [89]. It should be noted that there are inconsistencies in the literature regarding

conformational changes of FN and exposing its arginine-glycine-aspartic acid (RGD) motif. These reports have described that either hydrophilic or hydrophobic surfaces appear to undergo conformational changes of FN and exposing its RGD motif for integrin binding [89] [88]. According to other reports, the hydrophilic surfaces can expose FN's active cell-binding sites, resulting in higher integrin affinity and cell adhesion; in contrast, hydrophobic surfaces can strongly denature FN and disrupted its native structure [90–92]. In addition, FN that gains access to bare gold NPs undergoes significant unfolding with the formation of a hard corona; in contrast, corona-coated gold NPs maintain their original conformation via protein–protein interactions [93]. Therefore, it seems that there is a complex mechanism by which NP's surface features regulate the conformational changes of adsorbed proteins. Consequently, the surface features of CNPs with Ce-specific adsorbed proteins may be associated with a more complicated mechanism. For instance, when phosphates in body and cell culture buffers adsorb onto the surface of metal oxide NPs, such as titanium oxide (TiO_2) and iron oxide (α-Fe_2O_3) [94,95], the adsorbed phosphates may attenuate the adsorbed protein's denaturation and reduce its surface coverage [10]. This is due to the adsorbed phosphates blocking the active sites of the metal oxide NPs [10,94]. As for cerium oxide (CeO_2), the Ce^{3+}-CNPs readily adsorb phosphorus and phosphates [31,34]. In this context, the adsorbed phosphorous and phosphates on the Ce^{3+}-CNPs are likely to further reduce the surface coverage of Ce valence-specific proteins, including FN and LN. This corresponded to the present study's findings that the adsorbed amounts of FN and LN on Ce^{3+}-CNPs were significantly lower compared with that on Ce^{4+}-CNPs (Fig. 6b). It should be noted that the total amounts of proteins adsorbed on CNPs/PLs are independent on Ce valent states [31]. In addition, the surface chemistry of NPs and the pH of the surrounding solution are known to affect the structure of proteins on the corona [80]. For instance, under the acidic pH of a tumour microenvironment, the FN in the protein

corona is likely to undergo less unfolding, which may regulate the NP–cell interactions [93]. However, when the phosphorus/phosphate-adsorbed Ce^{3+}-CNPs are exposed in an acidic environment, the phosphorus/phosphates can desorb from the surface of Ce^{3+}-CNPs [33]. Therefore, reversibly adsorbed and desorbed phosphorus/phosphates on Ce^{3+}-CNPs appear to switch the probability of dynamic protein alterations, such as conformational changes and folding or unfolding of individual proteins in the corona, depending on the pH levels of the physiological and pathological environments (i.e. normal or tumour microenvironments). Further investigation is required: to identify the essential proteins to cue cells via receptor-mediated cell-NP interaction; and to clarify the dynamic conformational changes of adsorbed proteins and their corona structures on CNPs depending on pH levels. The present study's findings increase understanding of the non-redox mechanisms by which CNPs with Ce valence-specific novel functionalities selectively inhibit the growth of specific tumour cells for cancer treatment.

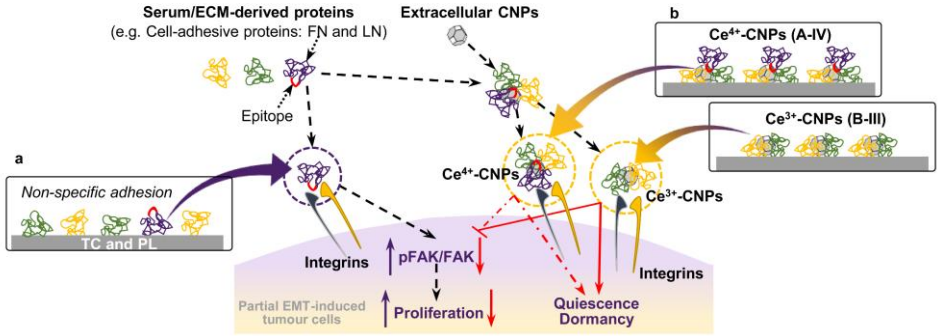

Fig. 8. Schematic drawings of possible cell-CNP interactions mediated by integrin ligation with protein coronas. Possible protein corona formation on **a.** TC and PL, **b.** CNPs/PLs with dominant Ce^{3+}/Ce^{4+} ions (i.e. Ce^{3+}-CNPs and Ce^{4+}-CNPs). Integrin interactions with proteins adsorbed on CNPs may lead to the inhibition of pFAK/FAK-derived cell proliferation and the cell cycle arrest at G0 phase (quiescence/dormancy).

5. Conclusions

This study demonstrated that extracellular CNPs selectively inhibited the growth of pEMT-induced tumour cells by causing a growth-arrested state without inducing redox-related ROS generation and apoptosis, i.e. non-redox mechanisms. Interestingly, the presence of dominant Ce^{3+} ions in extracellular CNPs provided *highly efficient* selective growth inhibition of pEMT-induced tumour cells, while that of dominant Ce^{4+} ions caused *highly selective and appropriate* growth regulation of normal mesenchymal and tumour epithelial/mesenchymal cell growth, leading to a reduction in treatment side effects. In addition, the physicochemical features of CNPs, such as cerium valence states, potentially influenced the conformational changes of adsorbed proteins and the structure of protein corona. The CNPs adsorbed with Ce valence-specific protein corona, including FN and LN, appeared to act as ligands to regulate the receptor-mediated cell-NP interaction. Therefore, the CNPs may acquire target-like capabilities to selectively inhibit the growth of pEMT-induced tumour cells. To further enhance the target-like capabilities of CNPs, identifying the essential proteins and their structures to cue cells could play an important role in the surface designs of nanomedicine to regulate desirable changes in the protein corona. Consequently, the biointerface of CNPs with Ce valence-specific protein corona may serve as a surface functionalisation of biomaterials and drug delivery vehicles to selectively inhibit the growth of pEMT-induced tumour cells, including cancer stem-like cells. Additionally, because extracellular CNPs did not interfere with fully epithelial tumour cells, the use of extracellular CNPs could offer the potential for combination therapy with standard anticancer drugs that target proliferative epithelial tumour cells. The present study's findings emphasise the probability of pEMT-targeting anticancer treatments based on the adaptive biointerface of extracellular NPs with metal valence-specific protein corona.

References

[1] I. Pastushenko, A. Brisebarre, A. Sifrim, M. Fioramonti, T. Revenco, S. Boumahdi, A. Van Keymeulen, D. Brown, V. Moers, S. Lemaire, S. De Clercq, E. Minguijón, C. Balsat, Y. Sokolow, C. Dubois, F. De Cock, S. Scozzaro, F. Sopena, A. Lanas, N. D'haene, I. Salmon, J.C. Marine, T. Voet, P.A. Sotiropoulou, C. Blanpain, Identification of the tumour transition states occurring during EMT, Nature. 556 (2018) 463–468. https://doi.org/10.1038/s41586-018-0040-3.

[2] S. Brabletz, H. Schuhwerk, T. Brabletz, M.P. Stemmler, Dynamic EMT: a multi-tool for tumor progression, EMBO J. 40 (2021) e108647. https://doi.org/10.15252/embj.2021108647.

[3] M.K. Jolly, M. Boareto, B. Huang, D. Jia, M. Lu, J.N. Onuchic, H. Levine, E. Ben-Jacob, Implications of the hybrid epithelial/mesenchymal phenotype in metastasis, Front Oncol. 5 (2015) 155. https://doi.org/10.3389/fonc.2015.00155.

[4] D. Sinha, P. Saha, A. Samanta, A. Bishayee, Emerging concepts of hybrid epithelial-to-mesenchymal transition in cancer progression, Biomolecules. 10 (2020) 1–22. https://doi.org/10.3390/biom10111561.

[5] C. Liao, Q. Wang, J. An, Q. Long, H. Wang, M. Xiang, M. Xiang, Y. Zhao, Y. Liu, J. Liu, X. Guan, Partial EMT in squamous cell carcinoma: A snapshot, Int J Biol Sci. 17 (2021) 3036–3047. https://doi.org/10.7150/ijbs.61566.

[6] A. Pal, T.F. Barrett, R. Paolini, A. Parikh, S. V Puram, Partial EMT in head and neck cancer biology: A spectrum instead of a switch, Oncogene. 40 (2022) 5049–5065. https://doi.org/10.1038/s41388-021-01868-5.Partial.

[7] S. V. Puram, I. Tirosh, A.S. Parikh, A.P. Patel, K. Yizhak, S. Gillespie, C. Rodman, C.L. Luo, E.A. Mroz, K.S. Emerick, D.G. Deschler, M.A. Varvares, R. Mylvaganam, O. Rozenblatt-Rosen, J.W. Rocco, W.C. Faquin, D.T. Lin, A. Regev, B.E. Bernstein, Single-Cell Transcriptomic Analysis of Primary and Metastatic Tumor Ecosystems in Head and Neck Cancer, Cell. 171 (2017) 1611-1624.e24. https://doi.org/10.1016/j.cell.2017.10.044.

[8] M.J. Mitchell, M.M. Billingsley, R.M. Haley, M.E. Wechsler, N.A. Peppas, R. Langer, Engineering precision nanoparticles for drug delivery, Nat Rev Drug Discov. 20 (2021) 101–124. https://doi.org/10.1038/s41573-020-0090-8.

[9] L. Sun, H. Liu, Y. Ye, Y. Lei, R. Islam, S. Tan, R. Tong, Y.B. Miao, L. Cai, Smart nanoparticles for cancer therapy, Signal Transduct Target Ther. 8 (2023). https://doi.org/10.1038/s41392-023-01642-x.

[10] D. Fan, Y. Cao, M. Cao, Y. Wang, Y. Cao, T. Gong, Nanomedicine in cancer therapy, Signal Transduct Target Ther. 8 (2023). https://doi.org/10.1038/s41392-023-01536-y.

[11] R.H. Fang, A. V. Kroll, W. Gao, L. Zhang, Cell Membrane Coating Nanotechnology, Adv Mater. 30 (2018) 1–34. https://doi.org/10.1002/adma.201706759.

[12] L. Chen, W. Hong, W. Ren, T. Xu, Z. Qian, Z. He, Recent progress in targeted delivery vectors based on biomimetic nanoparticles, Signal Transduct Target Ther. 6 (2021) 225. https://doi.org/10.1038/s41392-021-00631-2.

[13] N.M. Sakhrani, H. Padh, Organelle targeting: Third level of drug targeting, Drug Des Devel Ther. 7 (2013) 585–599. https://doi.org/10.2147/DDDT.S45614.

[14] X. Ma, N. Gong, L. Zhong, J. Sun, X.J. Liang, Future of nanotherapeutics: Targeting the cellular sub-organelles, Biomaterials. 97 (2016) 10–21. https://doi.org/10.1016/j.biomaterials.2016.04.026.

[15] S. Wilhelm, A. J. Tavares, Q. Dai, S. Ohta, J. Audet, H. F. Dvorak, W. C.W. Chan, Analysis of nanoparticle delivery to tumours, Nat Rev Mater. 1 (2016) 16014. https://doi.org/10.1038/natrevmats.2016.14.

[16] N. Bertrand, J. Wu, X. Xu, N. Kamaly, O.C. Farokhzad, The impact of passive and active targeting in the era of modern cancer biology, Cancer Nanotechnol. 66 (2014) 2–25. https://doi.org/10.1016/j.addr.2013.11.009.Cancer.

[17] E. Henke, R. Nandigama, S. Ergün, Extracellular Matrix in the Tumor Microenvironment and Its Impact on Cancer Therapy, Front Mol Biosci. 6 (2019) 160. https://doi.org/10.3389/fmolb.2019.00160.

[18] A. Nayak, N.M. Warrier, P. Kumar, Cancer Stem Cells and the Tumor Microenvironment: Targeting the Critical Crosstalk through Nanocarrier Systems, Stem Cell Rev Reports. 18 (2022) 2209–2233. https://doi.org/10.1007/s12015-022-10426-9.

[19] R. Baghban, L. Roshangar, R. Jahanban-Esfahlan, K. Seidi, A. Ebrahimi-Kalan, M. Jaymand, S. Kolahian, T. Javaheri, P. Zare, Tumor microenvironment complexity and therapeutic implications at a glance, Cell Commun Signal. 18 (2020) 1–19. https://doi.org/10.1186/s12964-020-0530-4.

[20] D. Jiang, D. Ni, Z.T. Rosenkrans, P. Huang, X. Yan, W. Cai, Nanozyme: New horizons for responsive biomedical applications, Chem Soc Rev. 48 (2019) 3683–3704. https://doi.org/10.1039/c8cs00718g.

[21] Y. Huang, J. Ren, X. Qu, Nanozymes: Classification, Catalytic Mechanisms, Activity Regulation, and Applications, Chem Rev. 119 (2019) 4357–4412. https://doi.org/10.1021/acs.chemrev.8b00672.

[22] E. Wei, Hui, Wang, Nanomaterials with enzyme-like characteristics (nanozymes): next-generation artificial enzymes, Chem Soc Rev. 42 (2013) 6060–6093. https://doi.org/10.1039/c3cs35486e.

[23] X. Fu, X. Yu, J. Jiang, J. Yang, L. Chen, Z. Yang, C. Yu, Small molecule-assisted assembly of multifunctional ceria nanozymes for synergistic treatment of atherosclerosis, Nat Commun. 13 (2022) 6528. https://doi.org/10.1038/s41467-022-34248-y.

[24] T.L. Nguyen, Y. Choi, J. Im, H. Shin, N.M. Phan, M.K. Kim, S.W. Choi, J. Kim, Immunosuppressive biomaterial-based therapeutic vaccine to treat multiple sclerosis via re-establishing immune tolerance, Nat Commun. 13 (2022) 7449. https://doi.org/10.1038/s41467-022-35263-9.

[25] H.J. Kwon, M.Y. Cha, D. Kim, D.K. Kim, M. Soh, K. Shin, T. Hyeon, I. Mook-Jung, Mitochondria-Targeting Ceria Nanoparticles as Antioxidants for Alzheimeŕs Disease, ACS Nano. 10 (2016) 2860–2870. https://doi.org/10.1021/acsnano.5b08045.

[26] Q. Weng, H. Sun, C. Fang, F. Xia, H. Liao, J. Lee, J. Wang, A. Xie, J. Ren, X. Guo, F. Li, B. Yang, D. Ling, Catalytic activity tunable ceria nanoparticles prevent chemotherapy-induced acute kidney injury without interference with chemotherapeutics, Nat Commun. 12 (2021) 1436. https://doi.org/10.1038/s41467-021-21714-2.

[27] F. Pagliari, C. Mandoli, G. Forte, E. Magnani, S. Pagliari, G. Nardone, S. Licoccia, M. Minieri, P. Di Nardo, E. Traversa, Cerium oxide nanoparticles protect cardiac progenitor cells from oxidative stress, ACS Nano. 6 (2012) 3767–3775. https://doi.org/10.1021/nn2048069.

[28] M.S. Wason, J. Colon, S. Das, S. Seal, J. Turkson, J. Zhao, C.H. Baker, Sensitization of pancreatic cancer cells to radiation by cerium oxide nanoparticle-induced ROS

production, Nanomedicine Nanotechnology, Biol Med. 9 (2013) 558. https://doi.org/10.1016/j.nano.2012.10.010.

[29] L. Alili, M. Sack, A.S. Karakoti, S. Teuber, K. Puschmann, S.M. Hirst, C.M. Reilly, K. Zanger, W. Stahl, S. Das, S. Seal, P. Brenneisen, Combined cytotoxic and anti-invasive properties of redox-active nanoparticles in tumor-stroma interactions, Biomaterials. 32 (2011) 2918–2929. https://doi.org/10.1016/j.biomaterials.2010.12.056.

[30] F. Corsi, F. Caputo, E. Traversa, L. Ghibelli, Not only redox: The multifaceted activity of cerium oxide nanoparticles in cancer prevention and therapy, Front Oncol. 8 (2018) 1–7. https://doi.org/10.3389/fonc.2018.00309.

[31] T. Naganuma, E. Traversa, The effect of cerium valence states at cerium oxide nanoparticle surfaces on cell proliferation, Biomaterials. 35 (2014) 4441–4453. https://doi.org/10.1016/j.biomaterials.2014.01.074.

[32] S. Singh, T. Dosani, A.S. Karakoti, A. Kumar, S. Seal, W.T. Self, A phosphate-dependent shift in redox state of cerium oxide nanoparticles and its effects on catalytic properties, Biomaterials. 32 (2011) 6745–6753. https://doi.org/10.1016/j.biomaterials.2011.05.073.

[33] T. Naganuma, Tunable phosphate-mediated stability of Ce^{3+} ions in cerium oxide nanoparticles for enhanced switching efficiency of their anti/pro-oxidant activities, Biomater Sci. 9 (2021) 1345–1354. https://doi.org/10.1039/d0bm01860k.

[34] T. Naganuma, E. Traversa, Air, aqueous and thermal stabilities of Ce^{3+} ions in cerium oxide nanoparticle layers with substrates, Nanoscale. 6 (2014) 6637–6645. https://doi.org/10.1039/c3nr06662b.

[35] M. Mahmoudi, M.P. Landry, A. Moore, R. Coreas, The protein corona from nanomedicine to environmental science, Nat Rev Mater. 8 (2023) 422–438. https://doi.org/10.1038/s41578-023-00552-2.

[36] A.E. Nel, L. Mädler, D. Velegol, T. Xia, E.M.V. Hoek, P. Somasundaran, F. Klaessig, V. Castranova, M. Thompson, Understanding biophysicochemical interactions at the nano-bio interface, Nat Mater. 8 (2009) 543–557. https://doi.org/10.1038/nmat2442.

[37] H. Mohammad-Beigi, Y. Hayashi, C.M. Zeuthen, H. Eskandari, C. Scavenius, K. Juul-Madsen, T. Vorup-Jensen, J.J. Enghild, D.S. Sutherland, Mapping and identification of soft corona proteins at nanoparticles and their impact on cellular association, Nat Commun. 11 (2020) 4535. https://doi.org/https://doi.org/10.1038/s41467-020-18237-7.

[38] M.P. Monopoli, C. Åberg, A. Salvati, K.A. Dawson, Biomolecular coronas provide the biological identity of nanosized materials, Nat Nanotechnol. 7 (2012) 779–786. https://doi.org/10.1038/nnano.2012.207.

[39] T. Naganuma, E. Traversa, Stability of the Ce^{3+} valence state in cerium oxide nanoparticle layers, Nanoscale. 4 (2012) 4950–4953. https://doi.org/10.1039/c2nr30406f.

[40] J.M. Lee, S. Dedhar, R. Kalluri, E.W. Thompson, The epithelial-mesenchymal transition: New insights in signaling, development, and disease, J Cell Biol. 172 (2006) 973–981. https://doi.org/10.1083/jcb.200601018.

[41] Y. Shintani, M. Maeda, N. Chaika, K.R. Johnson, M.J. Wheelock, Collagen I promotes epithelial-to-mesenchymal transition in lung cancer cells via transforming growth factor-β signaling, Am J Respir Cell Mol Biol. 38 (2008) 95–104. https://doi.org/10.1165/rcmb.2007-0071OC.

[42] Y. Shintani, M.A. Hollingsworth, M.J. Wheelock, K.R. Johnson, Collagen I promotes metastasis in pancreatic cancer by activating c-Jun NH2-terminal kinase 1 and up-regulating N-cadherin expression, Cancer Res. 66 (2006) 11745–11753. https://doi.org/10.1158/0008-5472.CAN-06-2322.

[43] V. Tirino, R. Camerlingo, K. Bifulco, E. Irollo, R. Montella, F. Paino, G. Sessa, M. V. Carriero, N. Normanno, G. Rocco, G. Pirozzi, TGF-β1 exposure induces epithelial to mesenchymal transition both in CSCs and non-CSCs of the A549 cell line, leading to an increase of migration ability in the CD133+ A549 cell fraction, Cell Death Dis. 4 (2013) e620. https://doi.org/10.1038/cddis.2013.144.

[44] T. Pirmohamed, J.M. Dowding, S. Singh, B. Wasserman, E. Heckert, A.S. Karakoti, J.E.S. King, S. Seal, W.T. Self, Nanoceria exhibit redox state-dependent catalase mimetic activity, Chem Commun. 46 (2010) 2736–2738. https://doi.org/10.1039/b922024k.

[45] E.G. Heckert, A.S. Karakoti, S. Seal, W.T. Self, The role of cerium redox state in the SOD mimetic activity of nanoceria, Biomaterials. 29 (2008) 2705–2709. https://doi.org/10.1016/j.biomaterials.2008.03.014.

[46] T. Naganuma, Shape design of cerium oxide nanoparticles for enhancement of enzyme mimetic activity in therapeutic applications, Nano Res. 10 (2017) 199–217. https://doi.org/10.1007/s12274-016-1278-4.

[47] R. Kumari, P. Jat, Mechanisms of Cellular Senescence: Cell Cycle Arrest and Senescence Associated Secretory Phenotype, Front Cell Dev Biol. 9 (2021) 646693. https://doi.org/10.3389/fcell.2021.645593.

[48] T.G. Phan, P.I. Croucher, The dormant cancer cell life cycle, Nat Rev Cancer. 20 (2020) 398–411. https://doi.org/10.1038/s41568-020-0263-0.

[49] S.K. Rehman, J. Haynes, E. Collignon, K.R. Brown, Y. Wang, A.M.L. Nixon, J.P. Bruce, J.A. Wintersinger, A. Singh Mer, E.B.L. Lo, C. Leung, E. Lima-Fernandes, N.M. Pedley, F. Soares, S. McGibbon, H.H. He, A. Pollet, T.J. Pugh, B. Haibe-Kains, Q. Morris, M. Ramalho-Santos, S. Goyal, J. Moffat, C.A. O'Brien, Colorectal Cancer Cells Enter a Diapause-like DTP State to Survive Chemotherapy, Cell. 184 (2021) 226-242.e21. https://doi.org/10.1016/j.cell.2020.11.018.

[50] A.J. Wiecek, S.J. Cutty, D. Kornai, M. Parreno-Centeno, L.E. Gourmet, G.M. Tagliazucchi, D.H. Jacobson, P. Zhang, L. Xiong, G.L. Bond, A.R. Barr, M. Secrier, Genomic hallmarks and therapeutic implications of cancer cell quiescence, Genome Biol. 24 (2022) 128. https://doi.org/10.1186/s13059-023-02963-4.

[51] I.J. Huijbers, M. Iravani, S. Popov, D. Robertson, S. Al-Sarraj, C. Jones, C.M. Isacke, A role for fibrillar collagen deposition and the collagen internalization receptor endo180 in glioma invasion, PLoS One. 5 (2010) e9808. https://doi.org/10.1371/journal.pone.0009808.

[52] T. Mammoto, A. Jiang, E. Jiang, D. Panigrahy, M.W. Kieran, A. Mammoto, Role of collagen matrix in tumor angiogenesis and glioblastoma multiforme progression, Am J Pathol. 183 (2013) 1293–1305. https://doi.org/10.1016/j.ajpath.2013.06.026.

[53] P.P. Provenzano, D.R. Inman, K.W. Eliceiri, J.G. Knittel, L. Yan, C.T. Rueden, J.G. White, P.J. Keely, Collagen density promotes mammary tumor initiation and progression, BMC Med. 6 (2008) 11. https://doi.org/10.1186/1741-7015-6-11.

[54] G.W. McLean, N.O. Carragher, E. Avizienyte, J. Evans, V.G. Brunton, M.C. Frame, The role of focal-adhesion kinase in cancer - A new therapeutic opportunity, Nat Rev Cancer. 5 (2005) 505–515. https://doi.org/10.1038/nrc1647.

[55] F.J. Sulzmaier, C. Jean, D.D. Schlaepfer, FAK in cancer: Mechanistic findings and clinical applications, Nat Rev Cancer. 14 (2014) 598–610. https://doi.org/10.1038/nrc3792.

[56] K. Brami-Cherrier, N. Gervasi, D. Arsenieva, K. Walkiewicz, M.C. Boutterin, A. Ortega, P.G. Leonard, B. Seantier, L. Gasmi, T. Bouceba, G. Kadaré, J.A. Girault, S.T. Arold, FAK dimerization controls its kinase-dependent functions at focal adhesions, EMBO J. 33 (2014) 356–370. https://doi.org/10.1002/embj.201386399.

[57] J.C. Dawson, A. Serrels, D.G. Stupack, D.D. Schlaepfer, M.C. Frame, Targeting FAK in anticancer combination therapies, Nat Rev Cancer. 21 (2021) 313–324. https://doi.org/10.1038/s41568-021-00340-6.

[58] V. Kostourou, T. Lechertier, L.E. Reynolds, D.M. Lees, M. Baker, D.T. Jones, B. Tavora, A.R. Ramjaun, G.M. Birdsey, S.D. Robinson, M. Parsons, A.M. Randi, I.R. Hart, K. Hodivala-Dilke, FAK-heterozygous mice display enhanced tumour angiogenesis, Nat Commun. 4 (2013) 2020. https://doi.org/10.1038/ncomms3020.

[59] S.N. Hochwald, C. Nyberg, M. Zheng, D. Zheng, C. Wood, N.A. Massoll, A. Magis, D. Ostrov, W.G. Cance, M. Vita, A novel small molecule inhibitor of FAK decreases growth of human pancreatic cancer, Cell Cycle. 8 (2016) 2435–2443. https://doi.org/10.4161/cc.8.15.9145.

[60] E.W. Thompson, S.H. Nagaraj, Transition states that allow cancer to spread, Nature. 556 (2018) 442–444. https://doi.org/10.1038/d41586-018-04403-x.

[61] L. Zhang, Y. Liao, L. Tang, MicroRNA-34 family: A potential tumor suppressor and therapeutic candidate in cancer, J Exp Clin Cancer Res. 38 (2019) 53. https://doi.org/10.1186/s13046-019-1059-5.

[62] M.A. Cortez, D. Valdecanas, X. Zhang, Y. Zhan, V. Bhardwaj, G.A. Calin, R. Komaki, D.K. Giri, C.C. Quini, T. Wolfe, H.J. Peltier, A.G. Bader, J. V. Heymach, R.E. Meyn, J.W. Welsh, Therapeutic delivery of mir-200c enhances radiosensitivity in lung cancer, Mol Ther. 22 (2014) 1494–1503. https://doi.org/10.1038/mt.2014.79.

[63] C. V. Pecot, R. Rupaimoole, D. Yang, R. Akbani, C. Ivan, C. Lu, S. Wu, H.D. Han, M.Y. Shah, C. Rodriguez-Aguayo, J. Bottsford-Miller, Y. Liu, S.B. Kim, A. Unruh, V. Gonzalez-Villasana, L. Huang, B. Zand, M. Moreno-Smith, L.S. Mangala, M. Taylor, H.J. Dalton, V. Sehgal, Y. Wen, Y. Kang, K.A. Baggerly, J.S. Lee, P.T. Ram, M.K. Ravoori, V. Kundra, X. Zhang, R. Ali-Fehmi, A.M. Gonzalez-Angulo, P.P. Massion, G.A. Calin, G. Lopez-Berestein, W. Zhang, A.K. Sood, Tumour angiogenesis regulation by the miR-200 family, Nat Commun. 4 (2013) 2427. https://doi.org/10.1038/ncomms3427.

[64] M.M. Faheem, N.D. Seligson, S.M. Ahmad, R.U. Rasool, S.G. Gandhi, M. Bhagat, A. Goswami, Convergence of therapy-induced senescence (TIS) and EMT in multistep carcinogenesis: current opinions and emerging perspectives, Cell Death Discov. 6 (2020) 51. https://doi.org/10.1038/s41420-020-0286-z.

[65] J.A. Ewald, J.A. Desotelle, G. Wilding, D.F. Jarrard, Therapy-induced senescence in cancer, J Natl Cancer Inst. 102 (2010) 1536–1546. https://doi.org/10.1093/jnci/djq364.

[66] S. Gavas, S. Quazi, T.M. Karpiński, Nanoparticles for Cancer Therapy: Current Progress and Challenges, Nanoscale Res Lett. 16 (2021) 173. https://doi.org/10.1186/s11671-021-03628-6.

[67] Y. Yao, Y. Zhou, L. Liu, Y. Xu, Q. Chen, Y. Wang, S. Wu, Y. Deng, J. Zhang, A. Shao, Nanoparticle-Based Drug Delivery in Cancer Therapy and Its Role in Overcoming Drug Resistance, Front Mol Biosci. 7 (2020) 1–14. https://doi.org/10.3389/fmolb.2020.00193.

[68] Y. Zhang, Q. Chen, Y. Zhu, M. Pei, K. Wang, X. Qu, Y. Zhang, J. Gao, H. Qin, Targeting inorganic nanoparticles to tumors using biological membrane-coated technology, MedComm. 3 (2022) 1–19. https://doi.org/10.1002/mco2.192.

[69] A. Dadwal, A. Baldi, R. Kumar Narang, Nanoparticles as carriers for drug delivery in cancer, Artif Cells, Nanomedicine Biotechnol. 46 (2018) 295–305. https://doi.org/10.1080/21691401.2018.1457039.

[70] H. Han, The effect of nanoparticle size on in vivo pharmacokinetics and cellular interaction, Nanomedicine Nanotechnology, Biol Med. 11 (2016) 673–692.

[71] V.P. Torchilin, Recent advances with liposomes as pharmaceutical carriers, Nat Rev Drug Discov. 4 (2005) 145–160. https://doi.org/10.1038/nrd1632.

[72] S.K. Hobbs, W.L. Monsky, F. Yuan, W.G. Roberts, L. Griffith, V.P. Torchilin, R.K. Jain, Regulation of transport pathways in tumor vessels: Role of tumor type and microenvironment, Proc Natl Acad Sci U S A. 95 (1998) 4607–4612. https://doi.org/10.1073/pnas.95.8.4607.

[73] H. Kang, S. Rho, W.R. Stiles, S. Hu, Y. Baek, D.W. Hwang, S. Kashiwagi, M.S. Kim, H.S. Choi, Size-Dependent EPR Effect of Polymeric Nanoparticles on Tumor Targeting, Adv Healthc Mater. 9 (2020) 1–8. https://doi.org/10.1002/adhm.201901223.

[74] W. Jia, Y. Wang, R. Liu, X. Yu, H. Gao, Shape Transformable Strategies for Drug Delivery, Adv Funct Mater. 31 (2021) 1–23. https://doi.org/10.1002/adfm.202009765.

[75] P. Decuzzi, B. Godin, T. Tanaka, S.Y. Lee, C. Chiappini, X. Liu, M. Ferrari, Size and shape effects in the biodistribution of intravascularly injected particles, J Control Release. 141 (2010) 320–327. https://doi.org/10.1016/j.jconrel.2009.10.014.

[76] M.A. Bruckman, L.N. Randolph, A. VanMeter, S. Hern, A.J. Shoffstall, R.E. Taurog, N.F. Steinmetz, Biodistribution, pharmacokinetics, and blood compatibility of native and PEGylated tobacco mosaic virus nano-rods and -spheres in mice, Virology. 449 (2014) 163–173. https://doi.org/10.1016/j.virol.2013.10.035.

[77] E. Blanco, H. Shen, M. Ferrari, Principles of nanoparticle design for overcoming biological barriers to drug delivery, Nat Biotechnol. 33 (2015) 941–951. https://doi.org/10.1038/nbt.3330.

[78] C. Kinnear, T.L. Moore, L. Rodriguez-Lorenzo, B. Rothen-Rutishauser, A. Petri-Fink, Form Follows Function: Nanoparticle Shape and Its Implications for Nanomedicine, Chem Rev. 117 (2017) 11476–11521. https://doi.org/10.1021/acs.chemrev.7b00194.

[79] J. Fang, W. Islam, H. Maeda, Exploiting the dynamics of the EPR effect and strategies to improve the therapeutic effects of nanomedicines by using EPR effect enhancers, Adv Drug Deliv Rev. 157 (2020) 142–160. https://doi.org/10.1016/j.addr.2020.06.005.

[80] G. Bashiri, M.S. Padilla, K.L. Swingle, S.J. Shepherd, M.J. Mitchell, K. Wang, Nanoparticle protein corona: from structure and function to therapeutic targeting, Lab Chip. 23 (2023) 1432–1466. https://doi.org/10.1039/d2lc00799a.

[81] A. Lesniak, F. Fenaroli, M.P. Monopoli, C. Åberg, K.A. Dawson, A. Salvati, Effects of the presence or absence of a protein corona on silica nanoparticle uptake and impact on cells, ACS Nano. 6 (2012) 5845–5857. https://doi.org/10.1021/nn300223w.

[82] F. Francescangeli, M.L. De Angelis, R. Rossi, A. Cuccu, A. Giuliani, R. De Maria, A. Zeuner, Dormancy, stemness, and therapy resistance: interconnected players in cancer evolution, Cancer Metastasis Rev. 42 (2023) 197–215. https://doi.org/10.1007/s10555-023-10092-4.

[83] A. Sistigu, M. Musella, C. Galassi, I. Vitale, R. De Maria, Tuning Cancer Fate: Tumor Microenvironment's Role in Cancer Stem Cell Quiescence and Reawakening, Front Immunol. 11 (2020) 2166. https://doi.org/10.3389/fimmu.2020.02166.

[84] Y. Ohta, M. Fujii, S. Takahashi, A. Takano, K. Nanki, M. Matano, H. Hanyu, M. Saito, M. Shimokawa, S. Nishikori, Y. Hatano, R. Ishii, K. Sawada, A. Machinaga, W. Ikeda, T. Imamura, T. Sato, Cell–matrix interface regulates dormancy in human colon cancer stem cells, 608 (2022) 784-794. https://doi.org/10.1038/s41586-022-05043-y.

[85] F.G.G. Jonathan Cooper, Integrin Signaling in Cancer: Mechanotransduction, Stemness, Epithelial Plasticity, and Therapeutic Resistance, Cancer Cell. 35 (2019) 347–367. https://doi.org/10.1016/j.ccell.2019.01.007.Integrin.

[86] A. Salvati, A.S. Pitek, M.P. Monopoli, K. Prapainop, F.B. Bombelli, D.R. Hristov, P.M. Kelly, C. Åberg, E. Mahon, K.A. Dawson, Transferrin-functionalized nanoparticles lose their targeting capabilities when a biomolecule corona adsorbs on the surface, Nat Nanotechnol. 8 (2013) 137–143. https://doi.org/10.1038/nnano.2012.237.

[87] S. Tenzer, D. Docter, J. Kuharev, A. Musyanovych, V. Fetz, R. Hecht, F. Schlenk, D. Fischer, K. Kiouptsi, C. Reinhardt, K. Landfester, H. Schild, M. Maskos, S.K. Knauer, R.H. Stauber, Rapid formation of plasma protein corona critically affects nanoparticle pathophysiology, Nat Nanotechnol. 8 (2013) 772–781. https://doi.org/10.1038/nnano.2013.181.

[88] S. Kumar, S.H. Parekh, Molecular control of interfacial fibronectin structure on graphene oxide steers cell fate, ACS Appl Mater Interfaces. 13 (2021) 2346–2359. https://doi.org/10.1021/acsami.0c21042.

[89] N.E. Muzzio, M.A. Pasquale, X. Rios, O. Azzaroni, J. Llop, S.E. Moya, Adsorption and Exchangeability of Fibronectin and Serum Albumin Protein Corona on Annealed Polyelectrolyte Multilayers and Their Consequences on Cell Adhesion, Adv Mater Interfaces. 6 (2019) 1900008. https://doi.org/10.1002/admi.201900008.

[90] M.H. Lee, P. Ducheyne, L. Lynch, D. Boettiger, R.J. Composto, Effect of biomaterial surface properties on fibronectin- α5β1 integrin interaction and cellular attachment, Biomaterials. 27 (2006) 1907–1916. https://doi.org/10.1016/j.biomaterials.2005.11.003.

[91] B.G. Keselowsky, A.J. García, Surface chemistry modulates integrin binding to direct cell adhesion and function, J Biomed Mater Res A. 66 (2003) 247-59. 10.1002/jbm.a.10537.

[92] P.A. Underwood, J.G. Steele, B.A. Dalton, Effects of polystyrene surface chemistry on the biological activity of solid phase fibronectin and vitronectin, analysed with monoclonal antibodies, J Cell Sci. 104 (1993) 793–803. https://doi.org/10.1242/jcs.104.3.793.

[93] M. Raoufi, M.J. Hajipour, S.M. Kamali Shahri, I. Schoen, U. Linn, M. Mahmoudi, Probing fibronectin conformation on a protein corona layer around nanoparticles, Nanoscale. 10 (2018) 1228–1233. https://doi.org/10.1039/c7nr06970g.

[94] Z. Xu, V.H. Grassian, Bovine serum albumin adsorption on TiO_2 nanoparticle surfaces: Effects of ph and coadsorption of phosphate on protein-surface interactions and protein structure, J Phys Chem C. 121 (2017) 21763–21771. https://doi.org/10.1021/acs.jpcc.7b07525.

[95] I.B. Ustunol, E.K. Coward, E. Quirk, V.H. Grassian, Interaction of beta-lactoglobulin and bovine serum albumin with iron oxide (α-Fe_2O_3) nanoparticles in the presence and absence of pre-adsorbed phosphate, Environ Sci Nano. 8 (2021) 2811–2823. https://doi.org/10.1039/d1en00388g.

Acknowledgements

A part of this work was supported by "Advanced Research Infrastructure for Materials and Nanotechnology in Japan (ARIM)" of the Ministry of Education, Culture, Sports, Science and Technology (MEXT). Proposal Number JPMXP1223NM5064. The author would like to thank Dr. Taro Takemura and Dr. Xianglan Li (Research Network and Facility Services Division, NIMS, Japan) for invaluable discussions including biological suggestions.

Supplementary Information

Selective inhibition of partial EMT-induced tumour cell growth by cerium valence states of extracellular ceria nanoparticles

Tamaki Naganuma[*]

** Research Center for Macromolecules and Biomaterials, National Institute for Materials Science, 1-1 Namiki, Tsukuba, Ibaraki, 305-0044, Japan. NAGANUMA.Tamaki@nims.go.jp; Tel: +81-298-60-4800. Fax: +81-298-60-4799*

Table S1. Chemical composition of CNPs.

Main	%
CeO_2	>99.8
Impurity elements	ppm
Na	7
Mg	24
Al	123
Si	290
Si	550
Cl	20
K	7
Ca	97
Ti	<10
Cr	<15
Mn	<6
Fe	224
Co	<9
Ni	<14
Cu	27
Zn	24

By X – ray Fluorescence: XRF and
Atomic Absorption Spectrometry: AAS

Table S2. Characteristics of CNP/PLs (A-IV and B-III). Percentages of dominant Ce valence states and surface charges of CNPs.

	Ce Valence states*	Surface charge**
A-IV	Tetravalence, Ce^{4+} (76%)	Negative
B-III	Trivalence, Ce^{3+} (75%)	Positive

*XPS, **zeta potential

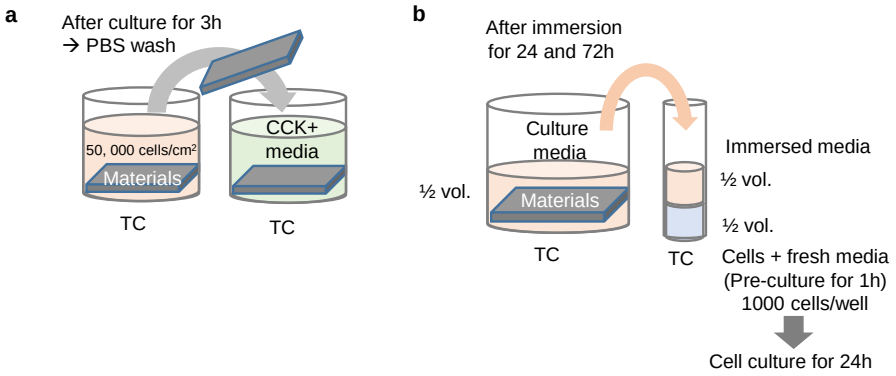

Fig. S1. Assay process conditions of a. high-dense cell adhesion onto CNP/PLs and b. cytotoxicity of possibly dissolved cerium ions.

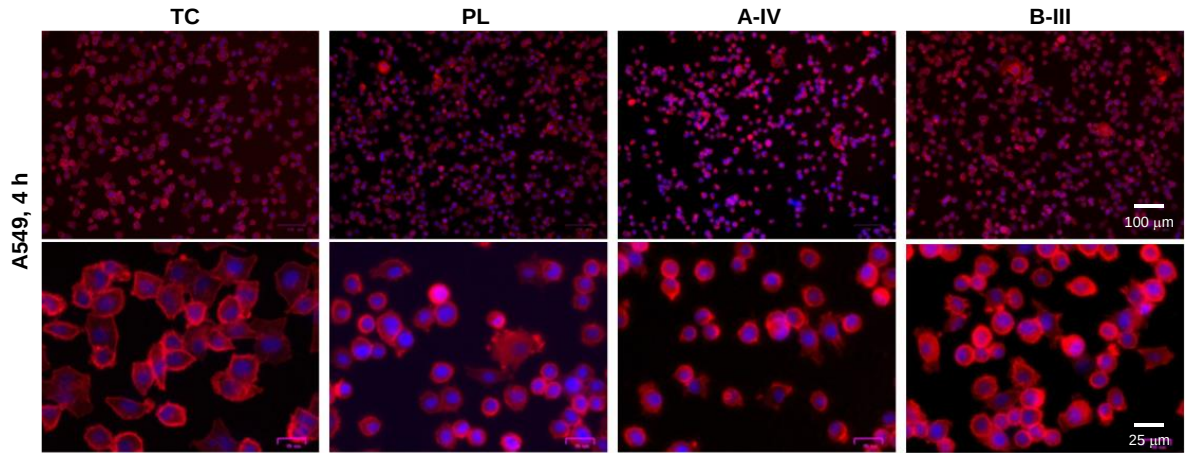

Fig. S2. Typical morphologies of A549 cells on each material at 4 h after seeding (red, actin; blue, nucleus) in high-dense cell adhesive assay (50,000 cells/cm^2).

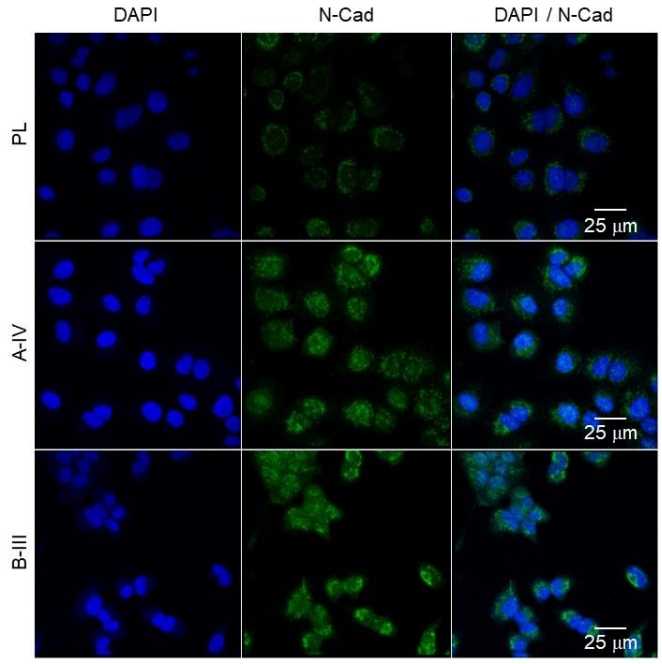

Fig. S3. Immunocytochemistry for N-cad (an EMT maker) in pEMT/A549 cells on PLs, A-IV and B-III at 72 h. N-cad is shown in green, and nuclei in blue.

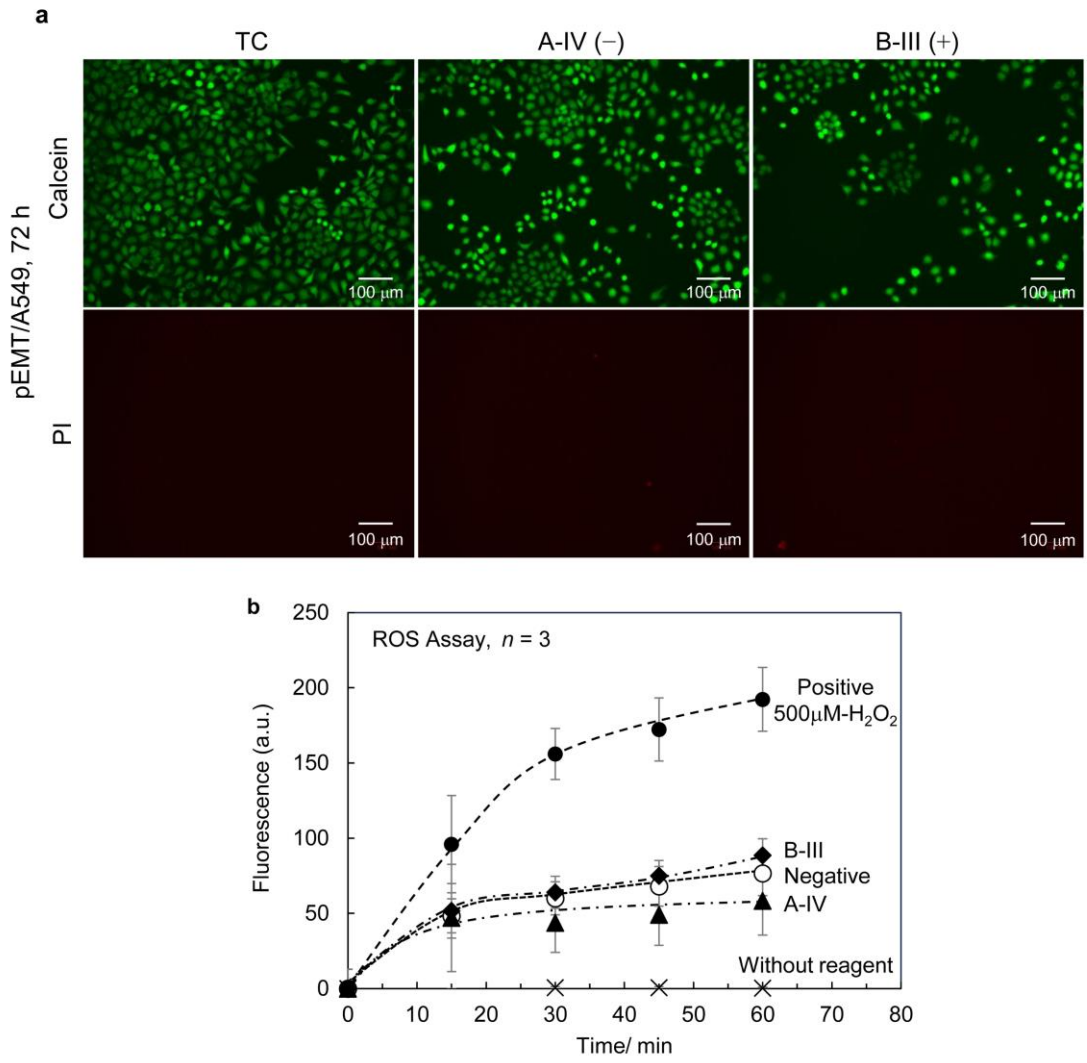

Fig. S4. a. Cell alive/death assay of pEMT/A549 cells on TC, negatively charged A-IV, and positively charged B-III at 72 h. b. Intercellular ROS Assay of pEMT/A549 cells on TC, A-IV and B-III. Treated cells with 500 μM-H_2O_2 were used as positive controls, and untreated cells were used as negative controls.